Single-nucleus analysis reveals dysregulated oxidative phosphorylation in Down syndrome basal forebrain at birth

Nicole R. West[1,2], Kalpana Hanthanan Arachchilage[1], Sara Knaack[1], Masoumeh Hosseini[1], Ryan D. Risgaard[1,2], Shawn MacGregor[1], Pubudu Kumarage[1], Jose L. Martinez[1], Daifeng Wang[1,3], Andre M.M. Sousa[1,4], Anita Bhattacharyya[1,5]*

[1]Waisman Center, University of Wisconsin-Madison, 1500 Highland Ave., Madison, WI 53705

[2]Cellular and Molecular Biology Graduate Program, University of Wisconsin-Madison, Bock Labs Room 413, 1525 Linden Dr., Madison, WI 53706

[3]Department of Biostatistics and Medical Informatics, University of Wisconsin-Madison School of Medicine and Public Health, WARF Room 201, 610 Walnut St., Madison, WI 53726

[4]Department of Neuroscience, University of Wisconsin-Madison School of Medicine and Public Health, WIMR II Room 5505, 1111 Highland Ave., Madison, WI 53705

[5]Department of Cell and Regenerative Biology, University of Wisconsin-Madison School of Medicine and Public Health, WIMR II Room 4403, 1111 Highland Ave., Madison, WI 53705

*Corresponding author: bhattacharyy@waisman.wisc.edu,

Waisman Center, University of Wisconsin-Madison, 1500 Highland Ave., Rm 623, Madison, WI 53705

Abstract:

INTRODUCTION: Basal forebrain cholinergic neurons (BFCNs) are integral to learning, attention, and memory, and are prone to degeneration in Down syndrome (DS), Alzheimer's disease, and other neurodegenerative diseases. However, the mechanisms that lead to degeneration of these neurons are not known.

METHODS: Single-nuclei gene expression and ATAC sequencing were performed on postmortem human basal forebrain from unaffected control and DS tissue samples at 0-2 years of age (n=4 each).

RESULTS: Sequencing analysis of postmortem human basal forebrain identifies gene expression differences in early postnatal DS early in life. Genes encoding proteins associated with energy metabolism pathways, specifically oxidative phosphorylation and glycolysis, and genes encoding antioxidant enzymes are upregulated in DS BFCNs.

DISCUSSION: Multiomic analyses reveal that energy metabolism may be disrupted in DS BFCNs by birth. Increased oxidative phosphorylation and the accumulation of reactive oxygen species byproducts may be early contributors to DS BFCN neurodegeneration.

1. Background

Cholinergic projection neurons of the basal forebrain (BFCNs), are the primary cholinergic input to the cortex, hippocampus, and amygdala, regulating cognitive functions including learning, attention, and memory[1]. The cholinergic hypothesis, proposed nearly 50 years ago, posits that the dysfunction or loss of cholinergic neurons

is an early driver of cognitive decline associated with age and Alzheimer's disease (AD)[2-4]. BFCNs are some of the first neurons to degenerate in the progression of AD[5-7]. Tau tangles accumulate in the basal forebrain in AD before the entorhinal cortex[5,6,8]. Studies suggest that BFCNs seed the cortex with pathology through the trans-synaptic spread of misfolded Tau[6,7]. Consequently, BFCNs have been a target of therapeutics to reduce degeneration, slow the spread of AD pathology, and ultimately to slow cognitive decline in AD[9,10]. Although the link between BFCN degeneration and memory decline is well understood, early molecular events that occur in BFCNs that increase susceptibility to degeneration later are unknown.

BFCN dysfunction and degeneration also occur in Down syndrome (DS, trisomy 21, T21)[11-15] and other neurodegenerative diseases, including Parkinson's disease (PD)[12,16-20] and Dementia with Lewy bodies (DLB)[21-24]. Nearly all individuals with DS develop AD (DS-AD), making DS the leading genetic cause of AD[25]. The progression of DS-AD pathology and the onset of dementia occurs in a consistent and predictable manner, enabling examination of successive stages of disease progression in DS[26,27]. BFCN degeneration in the anteromedial and posterior basal forebrain in individuals with DS begins about 30 years prior to the median onset of prodromal AD[14]. Post-mortem studies validated fewer neurons are present in the basal forebrain in DS relative to unaffected controls[11]. Further, DS is a neurodevelopmental disorder, and so we hypothesized that molecular changes early in life in DS BFCNs increase their susceptibility to degeneration. Identifying these molecular changes may provide insight into drivers of BFCN degeneration in the progression of DS-AD.

We performed unbiased single-nuclei gene expression and ATAC multiomic analysis of early human postnatal DS and unaffected control basal forebrain to identify molecular changes in DS that precede BFCN dysfunction or degeneration[14,28-30]. Our results suggest that energy metabolism, specifically the upregulation of glycolysis and oxidative phosphorylation (OXPHOS) genes, is dysregulated in DS BFCNs. Consequently, DS BFCNs have increased gene expression of antioxidant enzymes, possibly to regulate the reactive oxygen species (ROS) that accumulate as a byproduct of OXPHOS. The increased ROS over a sustained time may increase the vulnerability of DS BFCNs, causing their early degeneration in DS. These results identify potential novel targets for early therapeutic intervention that could delay BFCN dysfunction and mitigate disease progression.

2. Methods

2.1 Tissue Samples

Human basal forebrain post-mortem samples from Down syndrome and unaffected control individuals were obtained from the University of Maryland Brain and Tissue Bank, as part of the National Institutes of Health NeuroBioBank. Acquisition of the de-identified samples was approved by the Health Sciences Institutional Review Board at the University of Wisconsin-Madison (Protocol #2016-0979) and certified exempt from IRB oversight. Sample information is provided in **Figure 1A**.

2.2 Nuclei Isolation

Frozen post-mortem human basal forebrain (BF) tissue sections were pulverized into a powder in liquid nitrogen over dry ice, using a mortar and pestle (Fisherbrand, FB961A, FB961K). 25-35 mg of pulverized BF tissue was used for nuclei solation. All buffers were prepared fresh and maintained on ice. 3 mL of ice-cold buffer B (Iodixanol buffer) [50% (v/v) Optiprep (Iodixanol) solution (Sigma# D1556); 25 mM KCl (Sigma #60142); 5 mM MgCl2 (Sigma #M1028); 20 mM Tris-HCl (pH 7.5) (Invitrogen #15567-027); 1% cOmplete™, Mini, EDTA-free Protease Inhibitor Cocktail (Roche#11836170001); 1% BSA (GeminiBio #700-100p); RNase inhibitor (80U/mL) (Roche #03335402001); 1 mM DTT (Sigma #43186)] was transferred to a 15 mL tube.

1 mL buffer A (lysis buffer) [250 mM Sucrose (Sigma #S0389); 25 mM KCl2 (Sigma #21115); 5 mM MgCl2 (Sigma #63052); 20 mM Tris-HCl (pH 7.5) (Invitrogen #15567-027); 1% cOmplete™, Mini, EDTA-free Protease Inhibitor Cocktail (Roche#11836170001); RNase inhibitor (40U/mL) (Roche #03335402001); 1 mM DTT (Sigma #43186); 0.1 % (v/v) IGEPAL CA-630 (Sigma#I8896)] was added to the pulverized BF tissue in a tube. 1 mL of ice-cold lysis buffer was added to the Dounce tissue grinder (15 mL volume, Wheaton #357544; autoclaved, RNase free, ice-cold). 1 mL of lysis buffer was added to the pulverized tissue tube to rinse and collect all tissue. The suspension was transferred to Dounce tissue grinder and homogenized with loose and tight pestles, 30 cycles each, with constant pressure and without the introduction of air. The solution was transferred to the 15 mL tube containing buffer B and mixed by inverting the tube 10 times. The homogenate was filtered through a 40-um cell strainer (Falcon #352340) which was pre-washed with lysis buffer. Samples were centrifuged at

1000 g for 30 min at 4°C (Eppendorf #5910 Ri). Following centrifugation, the supernatant was carefully and completely removed and the pellet was resuspended in 1 mL of wash buffer [10 mM NaCl (Sigma #60142); 3 mM MgCl2 (Sigma #M1028); 10 mM Tris-HCl (pH 7.5) (Invitrogen #15567-027); 1% BSA (GeminiBio #700-100p); RNase inhibitor (1000U/mL) (Roche #03335402001); 1mM DTT (Sigma #43186)]. The homogenate was filtered through a 40-um cell strainer (Falcon #352340) pre-washed with wash buffer to eliminate large clumps and cell debris. Samples were then centrifuged at 500 g for 5 min at 4°C.

Supernatants were carefully and completely removed. Pellets were gently dissolved by adding 200 mL and 300 mL of buffer C [10 mM NaCl (Sigma #60142); 3 mM MgCl2 (Sigma #M1028); 10 mM Tris-HCl (pH 7.5) (Invitrogen #15567-027); 0.01% Tween-20 (Bio-Rad #1662404); 0.001% Digitonin (Thermo Fisher #BN2006); 0.01% (v/v) IGEPAL CA630 (Sigma#I8896); 1% cOmplete™, Mini, EDTA-free Protease Inhibitor Cocktail (Roche#11836170001); 1% BSA (GeminiBio #700-100p); RNase inhibitor (1000U/mL) (Roche #03335402001); 1mM DTT (Sigma #43186)].The solution was incubated on ice for 5 minutes. After incubation 500 mL of buffer D [10 mM NaCl (Sigma #60142); 3 mM MgCl2 (Sigma #M1028); 10 mM Tris-HCl (pH 7.5) (Invitrogen #15567-027); 0.1% Tween-20 (Bio-Rad #1662404); 1% BSA (GeminiBio #700-100p); RNase inhibitor (1000U/mL) (Roche #03335402001); 1mM DTT (Sigma #43186)) was added to the solution. After resuspension, nuclei quality was assessed at 40X magnification and were manually counted using a hemocytometer. The sample was centrifuged at 500 g for 5 min at 4°C. The pellet was resuspended in buffer E [1X nuclei buffer (10x

Genomics#2000207); RNase inhibitor (1000U/mL) (Roche #03335402001); 1mM DTT (Sigma #43186)] at a final concentration of 5 million nuclei/mL.

2.3 snMultiomic Library Generation and Sequencing

For each sample, 10,000 nuclei were targeted. Nuclei suspension was first incubated in a transposition mix. Thereafter, along with the oligo coated gel beads and partitioning oil (10x Genomics, PN-2000190), the single nuclei master mixture containing tagmented single nuclei suspension was transferred onto a Next GEM Chip J (10x Genomic, PN-2000264), and the chip was loaded to the Chromium Controller for GEM generation. After post GEM incubation clean up, preamplification of samples was performed and ATAC libraries were generated utilizing the Single Index Kit N Set A (10x Genomics, PN-1000212). The snRNA-seq libraries were generated using the Library Construction Kit (10x Genomics, PN-1000190) and Dual Index Kit TT Set A (10x Genomics, PN-1000215), following the manufacturer's recommended protocol. At each step, the concentration and quality of cDNA, ATAC library and GEX libraries were assessed by 4200 TapeStation (Agilent). Sequencing was carried out with Illumina NovaSeq X Plus for a targeted depth of 50,000 raw reads per nucleus.

2.4 snMultiomic Alignment

The 10x multiomic data was processed according to BICAN default methods. The snRNA-seq data were aligned with STAR v2.7.11a[31] and aggregated into count matrices with STARSolo. The alignments were performed locally using defaults from the WARP Multiome (v5.9.0) pipeline[32]. Initial quality control checks included assessment of the

percentages of uniquely- and multiply-mapped reads, and statistics of corrected barcodes and UMI. The snRNA-seq data alignment was done utilizing the GeneFull_Ex50pAS argument for STAR to ensure inclusion of alignments that overlap exonic ends within genic regions, in consideration of nuclear RNA processing biology.

The snATAC-seq data was likewise processed according to the WARP Multiome (v5.9.0) pipeline. This includes ibarcode correction with the fastqProcessing processing tool from WarpTools [32], and subsequent trimming with Cutadapt (v4.4)[33]. Alignment was performed with BWA-MEM2[34]. Finally, generation of fragment files and initial QC was performed with SnapATAC (v2.3.1)[35]. This was facilitated with an updated version of the snATAC component of the WARP Multiome (v5.9.0) pipeline to facilitate this workflow on Amazon AWS EC2 instances. Specifically, docker images for Cutadapt (v4.4) and for the BWA alignment were prepared to especially leverage AVX2 processing for improved performance. In this stage of the analysis all samples for either unaffected control or DS donors were treated identically.

2.5 snRNA-seq Processing and QC

Data processing and downstream analysis were conducted in R (4.4.0). Packages and versions are listed in **Supplement Table 1**. Due to the presence of an additional chromosome 21 in DS samples, the initial processing steps—quality control, preprocessing, batch correction, clustering, and cell type annotation—were conducted on control and DS samples separately. This approach was adopted for two reasons. First, during quality control, the upper threshold for the number of unique molecular identifiers (UMIs) was determined based on their lower and upper quartiles[36] (**Supplement 1A**).

Using a fixed cutoff for both control and DS samples would have been inappropriate due to the additional chromosome in DS samples. Second, identifying highly variable genes in a combined dataset (control and DS) would introduce a bias towards the effects of the additional chromosome, potentially obscuring signals differentiating cell type effects. Consequently, clustering and cell type annotations were performed separately.

The snRNA-seq datasets were preprocessed and analyzed using the Seurat (v5.1.0)[37,38] R package. mRNA contamination caused by cell-free ambient RNA in the gene expression data was corrected using the SoupX (v1.6.2)[39] package. Low-quality nuclei were then identified and removed based on stringent quality control thresholds: fewer than 200 expressed genes, ribosomal gene content exceeding 40%, mitochondrial gene content exceeding 5%, and a UMI count lower than 800 or higher than $Q_3 + 3(Q_3 - Q_1)$, where Q_1 and Q_3 are the lower and upper quartiles[36,40] (**Supplement 1A-B**). The upper UMI thresholds used were 29,284 in control and 34,160 in DS (**Supplement 1A**). After quality control, the datasets were subjected to doublet removal. Given the uncertainties inherent in doublet detection methods, an ensemble approach was employed, incorporating three techniques: DoubletFinder (v2.0.4)[41], Scrublet[42], and scDBIFinder v(1.18.0)[43]. A cell identified as a doublet by at least two of the three methods was classified as a doublet and removed from the dataset. Additional 'low quality cells' that could not confidently be identified with known marker genes were also removed (**Supplement 1C**). After all the quality control steps, the dataset retained a total of 37,467 cells (**Supplement 1D**). There is a positive correlation (0.92) between the number of unique molecular identifiers (RNA Count) and the number of genes (RNA Features) (**Supplement 1E**).

SoupX-corrected UMI counts were log-normalized using Seurat. The top 3,000 highly variable genes were identified using the default variance-stabilizing process. Gene expression data for these highly variable genes were then scaled, and dimensionality reduction was performed using principal component analysis (PCA). Batch effects were subsequently removed using Harmony (v1.2.3)[44] implemented within Seurat.

Clustering and cell type annotations were carried out in two steps. In the first step, Louvain clustering[38] was applied using the first 30 Harmony components with a cluster resolution of 0.5. Cell classes (e.g., neurons and non-neuronal cells) were assigned to the clusters based on the relative expression of a curated list of marker genes. In the second step, cells from each cell class were isolated and sub-clustered to identify more granular clusters representing specific cell subclasses and t-types based on a list of known marker genes (**Supplement Table 2**). This led to the identification of six non-neuronal subtypes: astrocytes, endothelial cells, microglia, oligodendrocytes, oligodendrocyte precursor cells (OPCs), and glial precursor cells (GPCs). GABAergic neurons were the only subclass of neurons identified, and BFCNs were identified as a t-type within the GABAergic population.

Following separate QC and cell annotations, control and DS data were combined and batch corrected using the Canonical Correlation Analysis (CCA) in Seurat. The FindMarkers() function in Seurat was used to identify differentially expressed genes (DEGs). Identified DEGs for each cell type are listed in **Supplement Table 3**. Hsa21 DEGs for each cell type are listed in **Supplement Table 4**. DEGs were mapped to chromosomes using the online tool, MG2C[45]. Gene Ontology analysis was performed with the online tool, Metascape[46] (v3.5.20240901).

2.6 snATAC-seq Processing and QC

The snATAC fragment data files were merged into a single master fragment file by 1) mapping the snATAC barcodes in the prepared per-sample fragment files to the corresponding snRNA seq barcodes (for direct integration), and 2) subsequently coordinate-sorting, compressing and tabulating these data for analysis in Seurat (v5.1.0)[37,38,47] and Signac (v1.14)[48]. The multiomic integration analysis proceeded by strategically assessing and filtering the snATAC data for those barcodes meeting the snRNA-seq quality control criteria.

Detailed QC assessment of the snATAC data for integration considered 1) number of fragments per barcode, 2) transcription start site (TSS) enrichment scores per barcode, and 3) nucleosome fraction scores per barcode for all putative multiomic analysis barcodes. Barcodes meeting the following criteria were selected for the integrated analysis: 1) number of fragments between 1k and 100k, 2) A TSS enrichment score >=2 and 3) nucleosome fraction score < 4 (**Supplement 4A-C**). QC selected 31,411 total barcodes for multiomic analysis (**Supplement 4D**).

2.7 Peak Calling

Peak calling was facilitated with the Signac CallPeaks() function, using MACS2 (v2.2.9.1)[49,50]. This was done for the integrated barcode data set partitioned by both annotated cell type (per the snRNA-seq analysis) and disease condition of donors (unaffected control and DS, respectively). For each cell type and condition, peaks were called, and a merged set of peak regions were compiled as implemented in CallPeaks().

A chromatin assay object representing the merged regions was aggregated by barcode and prepared in a merged Seurat object. The chief quality control measure assessed for the peak calling was the fraction of reads in peaks (FRiP) per barcode (**Supplement 4E**).

2.8 Peak-to-Gene Links

We estimated peak-to-gene links (i.e., nearby peaks correlated with gene expression of a given gene) for a few selected cell types to examine characteristics of regulatory elements across control and DS samples. These calculations were done separately across cell type and genotype. Peak-to-gene links within 500 kb of the corresponding transcription start sites (TSS) were obtained using LinkPeaks() function. The loci of genes of interest were then visualized using the coveragePlot() function in Signac, highlighting the differences in the regulatory landscape across control and DS samples.

3. Results

3.1 Overview of Human Basal Forebrain Tissue

Our data represent the first single sequencing of the human basal forebrain. Single-nuclei multiomic analysis of gene expression and chromatin accessibility (**Figure 1B**) was performed on four unaffected control and four DS basal forebrain samples matched for age, sex, and PMI (**Figure 1A**). After quality control (**Supplement 1A-C**), 34,467 cells were used for downstream analysis. Cells from all donors and ages were represented (**Figure 1C-D; Supplement 1D**). The cell types identified in the basal forebrain tissue samples were astrocytes, BFCNs, endothelial cells, GABAergic neurons,

glial progenitor cells (GPCs), microglia, oligodendrocytes, and oligodendrocyte precursor cells (OPCs) (**Figure 1E**). These results indicate that all expected cell types are present in all BF tissue samples.

3.2 Features of Control and DS Human Basal Forebrain

We assessed individual cell types in control and DS basal forebrain. Initially, cells were annotated by major cell class- excitatory neurons (ExN), inhibitory neurons (InN), and non-neuronal cells (NNC). Only InNs and NNCs were identified in the initial classification (**Supplement 2A**). NNCs and InNs were then independently sub-clustered to annotate subclasses. NNC subclasses were annotated as glial or endothelial cells (**Supplement 2B**). Astrocytes, GPCs, microglia, oligodendrocytes, and OPCs were the subtypes annotated in the glial subclass (**Figure 2A**). All InNs were annotated at the subclass level as GABAergic neurons (**Supplement 2B**). BFCNs were identified as a subtype within the GABAergic subclass (**Figure 2A**). BFCNs, which are capable of co-transmitting ACh and GABA[51,52], were initially annotated as InNs based on their expression of *GAD1, GABBR1,* and *SLC6A1* (**Supplement 2A-B**). While all cell types are present in both control and DS, the proportion of each cell type differs (**Figure 2A**). Proportional to total cell number, there are fewer astrocytes and more GABAergic neurons and microglia in the DS basal forebrain (**Figure 2A**). Following Canonical Correlation Analysis (CCA) integration, cell types from control and DS cluster together (**Supplement 2C**).

Principal component analysis (PCA) of pseudobulk data, categorized by cell type and genotype, reveals that cell-type identity, not genotype, has the greatest influence on gene expression (**Figure 2B**). Non-neuronal cells from the glial lineage (astrocytes,

GPCs, microglia, oligodendrocytes and OPCs) cluster closely together. The non-neuronal endothelial cells of the vasculature cluster separate from the other subtypes. GABAergic neurons and BFCNs cluster together (**Figure 2B**). The differences in gene expression that exist due to genotype are not enough to cause control and DS to form distinct clusters in the PCA plot. At the transcriptomic level, DS cells of the BF are, for the most part, similar to control BF cells at birth.

In all cell types, differentially expressed genes (DEGs) in DS compared to control are encoded across the genome (**Figure 2C; Supplement 2D-K; Supplement Table 3**), consistent with other gene expression data from DS[53-60]. Hsa21 genes (**Supplement Table 4**) account for a small percentage of DEGs in each cell type (**Supplement 2D-H**). Astrocytes have the most DEGs, followed by GABAergic neurons, oligodendrocytes, microglia, and BFCNs with the fewest DEGs (**Figure 2C**). While no DEGs are shared between all five cell types, several DEGs are shared between two or three cell types. Notably, almost half of DEGs in BFCNs are shared with both astrocytes and GABAergic neurons (**Supplement 2L**).

KEGG pathway analysis of the DEGs in each cell type reveals that genes in 'Glycolysis and Gluconeogenesis' pathways are enriched in BFCNs relative to the other cell types (**Figure 2D**). Neurons rely heavily on OXPHOS for ATP production because of their high energy demand and a shift toward glycolysis is indicative of mitochondrial dysfunction[61]. The enrichment of genes involved in 'Glycolysis and Gluconeogenesis' pathways in BFCNs relative to other cell types suggests mitochondrial dysfunction in BFCNs. This dysregulation of energy metabolism may be primarily driven by DS BFCNs.

3.3 Hsa21-Encoded Genes

We investigated whether and how Hsa21 genes are dysregulated in DS in five cell types: astrocytes, BFCNs, GABAergic neurons, microglia, and oligodendrocytes. Of the 221 predicted Hsa21 protein-coding genes annotated in the GRCh38.p14 reference assembly (https://www.ncbi.nlm.nih.gov/datasets/genome/GCF_000001405.40/), 56 Hsa21 genes are dysregulated in these cell types, with some genes dysregulated in more than one cell type (**Figure 3A; Supplement Table 4**). Hsa21 genes represent 1.66% of astrocyte DEGs, 5.56% of BFCN DEGs, 1.89% of GABAergic neuron DEGs, 3.70% of microglia DEGs, and 2.61% of oligodendrocyte DEGs (**Figure 3B; Supplement 2D-GH**). Thirty-one Hsa21 genes are upregulated in DS astrocytes (**Figure 3C**); 11 are upregulated in DS BFCNs (**Figure 3D**); 19 are upregulated in DS GABAergic neurons (**Figure 3E**); 4 are upregulated and 2 are downregulated in DS microglia (**Figure 3F**); 8 are upregulated and 2 are downregulated in DS oligodendrocytes (**Figure 3G**). These dysregulated Hsa21 genes account for 14.03%, 4.98%, 8.60%, 2.71%, and 4.52% of total Hsa21 protein-coding genes, respectively (**Figure 3H**). Fifty-five Hsa21 genes are dysregulated in endothelial cells, GPCs, and OPCs (**Supplement 3A-D**), accounting for 11.31%, 9.95%, and 15.38% of total Hsa21 protein-coding genes, respectively (Supplement 3E). With the exception of a few Hsa21 genes shared by multiple subtypes, most Hsa21 DEGs are unique to individual subtypes (**Figure 3A, 3C-G; Supplement 3A-D**), indicating Hsa21 gene dysregulation is intrinsic to each subtype. Interestingly, *PCP4* is upregulated in DS BFCNs, GABAergic neurons, microglia, oligodendrocytes, and endothelial cells (**Figure 3D-G; Supplement 3B**). The dysregulated Hsa21 genes are not enriched in any KEGG pathway. Despite the extra copy of Hsa21 genes in DS, Hsa21

genes constitute a small percentage of total DEGs between control and DS. Our results do not reveal specific Hsa21 genes that may be primary drivers of cellular dysfunction in the DS basal forebrain at birth.

3.4 Chromatin Accessibility of Hsa21 Genes

We assessed differences in chromatin accessibility and peak-to-gene linkages of Hsa21-encoded genes that could account for differential gene expression in the DS basal forebrain. Following QC of the ATAC-seq data (**Supplement 4A-C**), 16,771 control cells and 14,640 DS cells were used for downstream analysis (**Supplement 4D**). The integrated multiomic data was clustered, revealing that all cell types passed ATAC QC and were present in both control and DS samples (**Figure 4A**). However, the number of BFCNs that passed ATAC QC was too low to calculate any statistically significant peak-to-gene linkages in these cells. Two genes per subtype were selected from the Hsa21 DEGs to calculate peak-to-gene linkages (**Figure 3**). In DS astrocytes, larger peaks are present at the TSS of *DSCAM* and *S100B* (**Figure 4B**). DS GABAergic neurons have larger peaks at the TSS of *PCP4* and *SOD1* (**Figure 4C**). *EVA1C* and *S100B* have larger peaks at the TSS of DS microglia (**Figure 4D**). TSS peaks in *FTCD* and *IFNGR2* are increased in DS oligodendrocytes (**Figure 4E**). Since peaks mark regions of accessible chromatin, peaks near the TSS in the promoter region suggest increased chromatin accessibility, facilitating the recruitment of transcription factors and enhancers, which in turn promote active gene transcription. The peak-to-gene links observed in *DSCAM* and *S100B* (DS astrocytes), *PCP4* (DS GABAergic neurons), *EVA1C* and *S100B* (DS microglia), and *FTCD* (DS oligodendrocytes) may provide insight into potential gene

regulatory elements that control expression of these genes in DS (**Figure 4B-E**). Future work identifying these potential regulatory motifs and determining their necessity for gene regulation will provide further insight into the mechanisms controlling the expression of these genes in DS.

3.5 Non-Neuronal Cells

Recently, there has been an increased focus the important role of glial cells in neurodegenerative diseases, including DS[62,63]. We analyzed the differential gene expression in astrocytes, microglia, and oligodendrocytes to identify signatures of early deficits in glial cells of the DS basal forebrain. All glial cell subclasses (astrocytes, GPCs, microglia, oligodendrocytes, and OPCs) are present in both control and DS (**Figure 5A**) and were identified using known marker genes (**Supplement 5A; Supplement Table 2**). The proportion of astrocytes is decreased and the proportion of microglia is increased in DS relative to total glial cells (**Figure 5A**) and total cells (**Figure 2A**). The differential proportions of these cells are the first difference we identified in DS BF and may have functional consequences on both development and degeneration in the BF.

Identification of DEGs in DS astrocytes (log fold change, LFC>|1.5|, adjusted $P<.05$) revealed dysregulated genes across the genome, with a majority of the DEGs upregulated (**Supplement 2D; Supplement 5B; Supplement Table 3**). Hsa21 genes are represented at a slightly higher percentage in DS astrocytes when normalizing the DEGs per chromosome to the number of protein-coding genes of the chromosome (**Figure 5B**). The top 30 DEGs (from the largest absolute values of the LFCs) in DS astrocytes are all upregulated genes (**Figure 5B**) and all upregulated genes are enriched

for the GO term ‘Cellular Process’ (**Supplement 5C**). KEGG analysis reveals that genes in DS astrocytes are enriched in ‘Regulation of Actin Cytoskeleton’ and ‘Fc Gamma R-Mediated Phagocytosis’ (**Figure 5C**). The dysregulation of cytoskeletal regulation genes and genes involved in phagocytosis suggests that DS astrocytes are phagocytosing debris in the BF in an attempt to maintain tissue homeostasis.

DEGs (LFC>|1.5|, adjusted *P*<.05) in DS microglia are encoded across the genome, with approximately 2/3 DEGs upregulated in DS microglia (**Supplement 2G; Supplement 5D; Supplement Table 3**). Hsa21-encoded genes are also represented at a slightly higher percentage in DS microglia when accounting for the number of protein-coding genes per chromosome (**Figure 5D**). The top 30 DEGs in DS microglia comprised of 21 upregulated genes and 9 downregulated genes (**Figure 5D**). Genes upregulated in DS microglia are highly enriched for the GO terms ‘Cellular Process’ and ‘Immune System Process’ (**Supplement 5E)**. KEGG analysis reveals that genes dysregulated in DS microglia are enriched in the ‘Leishmania Infection’ pathway, which includes genes involved in antigen presentation, phagocytosis, and cytokine signaling. The enrichment of genes in the ‘B Cell Receptor Signaling Pathway’ and ‘FC Epsilon RI Signaling Pathway’ in control microglia suggests these pathways may be involved in maintaining microglial function (**Figure 5E**). These results indicate that, at birth, there is evidence of an immune response and dysregulation of microglial function in the DS basal forebrain.

In oligodendrocytes, DEGs (LFC>|1.5|, adjusted *P*<.05) are encoded across the genome, with most DEGs downregulated in DS (**Supplement 2H; Supplement 5F; Supplement Table 3**). Similar to the other glial cells, Hsa21 genes are represented at a slightly higher percentage in DS oligodendrocytes when normalizing DEGs to the

chromosome's number of protein-coding genes (**Figure 5F**). The top 30 DEGs include 28 downregulated and 2 upregulated genes in DS oligodendrocytes (**Figure 5F**). Genes downregulated in DS oligodendrocytes are enriched for the GO terms 'Cellular Process' and 'Response to Stimulus' (**Supplement 5G)**. Related to the dysregulated pathways of energy metabolism in other cells, KEGG pathway analysis suggests that the OXPHOS pathway is less active in DS oligodendrocytes (**Figure 5G**). These results may suggest that DS oligodendrocytes have reduced energy metabolism and may not be as responsive to the environmental cues, potentially contributing to the reduced myelination reported in DS [55,64,65].

3.6 GABAergic Neurons

To identify the BFCNs for downstream analysis, we sub-clustered the GABAergic neurons and annotated BFCN clusters based on known markers (**Figure 6A; Supplement 6A-B; Supplement Table 2**). GABAergic neurons account for ~10% of control cells and ~35% of DS cells in our data (**Figure 2A; Supplement 2C**). Of the total GABAergic neurons in control and DS, BFCNs comprise 5.17% and 2.38%, respectively (**Figure 6A**). snRNA-seq provides an unbiased approach to identify potential novel markers for BFCNs. However, relative to GABAergic neurons, many of the top BFCN marker genes have already been characterized or exhibit low levels of expression (**Figure 6B; Supplement 6C**).

DS GABAergic neurons have DEGs (LFC>|1.5|, adjusted P<.05) distributed across the genome (**Figure 2C; Supplement 2F**). Hsa21 genes make up a small percentage of DS GABAergic DEGs (**Figure 3B; Supplement 2F**) but are slightly more represented

when normalizing the DEGs per chromosome to the number of chromosome protein-coding genes (**Figure 6C**). Most dysregulated DEGs in DS GABAergic neurons are overexpressed (**Figure 6D; Supplement 2F**). The top 30 DEGs in DS GABAergic neurons based on the absolute value of the LFC are all upregulated genes (**Figure 6E**). KEGG pathway analysis reveals that DEGs in DS GABAergic neurons are enriched for genes encoding ribosomal subunits and components of the OXPHOS pathway, and DEGs are also associated with Alzheimer's disease (**Figure 6F**).

DS BFCNs also have DEGs (LFC>|1.25|, adjusted $P<.05$) distributed across the genome (**Figure 2C; Supplement 2E**) with Hsa21 genes comprising only 5.56% of DS BFCN DEGs (**Figure 3B; Supplement 2E**). However, Hsa21 genes are represented at a slightly higher percentage when normalizing DEGs to the number of chromosome protein-coding genes (**Figure 6G**). Most dysregulated DEGs in DS BFCNs are overexpressed (**Figure 6H; Supplement 2E**). The top 30 DEGs in DS BFCNs include 29 upregulated genes and one downregulated gene (**Figure 6I**). DEGs in DS BFCNs are enriched for genes encoding subunits in the OXPHOS pathway and are associated with Huntington's disease and Parkinson's disease (**Figure 6J**). Increased energy metabolism, specifically OXPHOS, may increase the production and accumulation of ROS in DS neurons, making them susceptible to degeneration. At these early postnatal ages, neurons in the DS basal forebrain already display dysregulation of genes associated with several neurodegenerative diseases.

3.7 Two Distinct BFCN Populations

When sub-clustering the GABAergic neurons, BFCNs separated into two clusters (**Figure 6A**). We then subset the BFCNs and sub-clustered them, again resulting in the separation of two distinct clusters (**Figure 7A**). The two clusters were annotated as BFCNs 1 and BFCNs 2. In controls these two populations of BFCNs are roughly equal in proportion whereas in DS there is a larger proportion of BFCNs 1 (**Figure 7A**).

We compared the expression of known BFCN markers in these two populations to identify their differences. Both BFCN populations express the established marker genes of BFCNs, including genes encoding enzymes and transporters in the acetylcholine (ACh) pathway (*CHAT, ACHE*, *SLC18A3, SLC5A7)*, neurotrophic receptors required for the maintenance and survival of BFCNs (*NTRK1, NGFR*), and transcription factors that regulate these genes (*ISL1, LHX8*). However, BFCNs 2 express the majority of these genes at lower levels compared to BFCNs 1 (**Figure 7B; Supplement 7A**). BFCNs 2 show a significant reduction in the expression of *SLC18A3,* a transmembrane protein responsible for transporting ACh into secretory vesicles for release, and *ACHE*, which hydrolyzes ACh into choline that is recycled for continued ACh synthesis (Figure 7B). These results suggest that BFCNs 2, with reduced expression of essential components for ACh neurotransmission, are likely not fully functional.

Given the young ages of the samples and the reduced expression of genes in the ACh pathway, we suspected that BFCNs 2 are a more immature population compared to BFCNs 1. Therefore, we assessed the expression of immature and mature neuron markers in these two populations (**Figure 7C**). Compared to BFCNs 1, BFCNs 2 have increased expression of *DCX*, an immature neuron marker (**Figure 7C**). Additionally,

BFCNs 2 exhibit decreased expression of the GABA receptors *GABBR1* and *GABBR2* along with decreased *GAD1* expression, which encodes GAD65, the enzyme that catalyzes the conversion of glutamate into GABA (**Figure 7C**). Differentially expressed genes calculated between BFCNs 1 and BFCNs 2 reveal that several tubulin genes and several genes involved in energy metabolism are upregulated in BFCNs 1 (**Figure 7D**). KEGG pathway analysis suggests that BFCNs 1 are likely more metabolically active, characteristic of more mature neurons, with upregulated genes in these cells enriched in 'Oxidative Phosphorylation' and 'Glycolysis and Gluconeogenesis' pathways (**Figure 7E**). The increased expression of *DCX*, the reduced expression of genes in the ACh and GABA pathways, and the reduced metabolic activity support that BFCNs 2 are a more immature population of cells.

Next, we compared the DEGs (LFC>|1.25|, adjusted $P<.05$) between DS and control in both BFCN populations. BFCNs 1 have 49 dysregulated genes between control and DS (**Figure 7F; Supplement 7B; Supplement Table 3**). Similar to the other subtypes, the percentage of Hsa21-encoded genes is slightly increased relative to protein-coding genes in BFCNs 1 (**Figure 7G; Supplement Table 4**). BFCNs 2 only have five DEGs between control and DS (**Figure 7H; Supplement 7B-D; Supplement Table 3**). No Hsa21 genes are dysregulated in BFCNs 2 (**Figure 7I; Supplement 7D-F**). No DEGs between control and DS are shared by BFCNs 1 and BFCNs 2 (**Supplement 7B**). PCA of the BFCN subpopulations shows that between control and DS, there is greater variability in the BFCNs 1 population (**Figure 7J)**. Control and DS BFCNs 1 separate from each other on the PCA plot whereas control and DS BFCNs 2 cluster close together

(Figure 7J). The limited number DEGs in DS BFCNs 2 precludes pathway analysis and so further analysis was performed only on the BFCNs 1 population.

3.8 Analysis of Mature BFCNs

We analyzed the DEGs (LFC>|1.25|, adjusted *P*<.05) of BFCNs 1 to understand the cellular mechanisms that may contribute to DS BFCN degeneration so early in life. Differentially expressed genes in BFCNs are less widely distributed across the genome compared to other cell types with no DEGs encoded on chromosomes 6, 7, 9, 13, 18, 20, or 22 (**Supplement 8A**). DS BFCNs have 48 upregulated genes and one downregulated gene relative to control (**Supplement 8B-C**). Of the top 30 DEGs in DS BFCNs, almost all upregulated (**Figure 8A; Supplement Table 3**). Genes upregulated in DS include those encoding subunits of the oxidative phosphorylation pathway (*NDUFS2, COX5A, ATP5PO,* and *UQCRC2),* antioxidant enzymes (*SOD1* and *PRDX2)*, and subunits of the vacuolar-type ATPase (V-ATPase) (*ATP6V0B, ATP6V0D1,* and *ATP6V0C)* (**Figure 8A; Supplement Table 3**). Overexpression of V-ATPase, an ATP-driven proton pump that regulates cellular pH and plays a role in overall cell homeostasis, has been linked to several human diseases[66]. Additionally, genes associated with glycolysis (*PGAM1, LDH8, LDHA, PDHA1,* and *PGK1*) are also upregulated in DS BFCNs (**Figure 8A; Supplement Table 3**). The increased expression of glycolysis-associated genes suggests a shift toward glycolysis as the primary source for energy production in DS BFCNs, a shift that is linked to mitochondrial dysfunction and several neurodegenerative diseases[61]. Although several genes related to energy metabolism are dysregulated in DS BFCNs, potential compensatory mechanisms may be at play, evidenced by the increased

expression of antioxidant enzymes and V-ATPase subunits, which help maintain cellular homeostasis.

GO term enrichment analysis reveals that upregulated genes in DS BFCNs are enriched for ‘Cellular Process’ and ‘Homeostatic Process’ categories (**Figure 8B**). KEGG enrichment analysis reveals that DS BFCN DEGs are enriched in the ‘Oxidative Phosphorylation’ pathway (**Figure 8C**), suggesting that DS BFCNs are more metabolically active than control BFCNs. Category Network Analysis (CNA) on genes upregulated in DS BFCNs revealed that, in addition to ‘Oxidative Phosphorylation’ and ‘Glycolysis/Gluconeogenesis’, these upregulated genes are significantly associated with several neurodegenerative diseases, including AD, PD, Huntington’s disease, Prion disease, and Amyotrophic lateral sclerosis (**Figure 8D**). Energy metabolism in DS BFCNs is dysregulated from an early age and may contribute to the susceptibility of BFCNs later in life.

While we lacked sufficient numbers of BFCNs to analyze statistically significant peak-to-gene linkages, we analyzed the BFCN ATAC-seq data to determine if chromatin accessibility of these genes varied between control and DS. The ATAC-seq analysis suggests differential chromatin accessibility at the TSS of *ATP6V0C* and *PRDX2* in DS BFCNs (**Figure 8E**). The increased chromatin accessibility suggests that the elevated expression of *ATP6V0C* and *PRDX2* in DS BFCNs results from enhanced transcriptional activation of these genes. *SOD1,* an Hsa21 gene, does not have differential chromatin accessibility at the TSS (**Figure 8E**). Increased gene expression without accompanying chromatin accessibility suggests that gene activation may be driven by regulatory

elements beyond chromatin structure. These could include enhancers, transcription factor binding, epigenetic modifications, or post-transcriptional regulation.

4. Discussion:

The organization of cholinergic neurons into four nuclei (Ch1-4) whose anatomical boundaries are not discrete[67,68], limits our ability to determine in which nucleus or nuclei the cholinergic neurons we analyzed reside. However, degeneration of the anteromedial basal forebrain (Ch1-3) and posterior basal forebrain (Ch4) occurs concomitantly in DS[14], so any changes likely apply to BFCNs from all nuclei.

Cholinergic neurons in the basal forebrain degenerate early in the course of disease progression in DS, AD, PD, and DLB. In DS, BFCNs degenerate beginning in the third decade of life[14], earlier than in other neurodegenerative disorders, yet there has been limited analysis of the human DS basal forebrain. Previous studies have examined the basal forebrain cholinergic system in DS and DS-AD, however, the youngest individuals in these studies are adolescents and young adults[11,14], ages when AD pathology has already begun to accumulate[26,27]. We sought to identify molecular signatures defining vulnerability that occur in DS prior to cholinergic dysfunction[28-30]. We sequenced and analyzed gene expression and ATAC data from the early postnatal basal forebrain of four control and four DS samples matched for age, sex, and PMI.

Results from our study reveal that basal forebrain pathology is evident as early as birth in DS, suggesting pathological processes begin prenatally. Our data provide the first gene expression and chromatin accessibility analysis of the human basal forebrain

cholinergic system from either healthy or diseased individuals, and thus establishes a rich resource for further investigation of neurodegeneration in this area.

All expected cell types are present in both control and DS early postnatal DS basal forebrain, but cell type proportions are altered in DS. These results suggest that prenatal development of the basal forebrain may be altered in DS, leading to the generation of different numbers of progenitors and/or neurons or, alternatively, that degeneration begins prenatally. Analysis of prenatal DS tissue and induced pluripotent stem cell studies are needed to interrogate earlier developmental time periods to test these possibilities. Interestingly, the proportions of neurons and glia are contrary to reports in the DS cortex, where neurons are reduced, and astrocytes are increased compared to controls[69-71].

We identified molecular events that occur in DS prior to cholinergic dysfunction[28-30] that provide clues to the vulnerability of BFCNs. We uncovered dysregulation of genes in all cell types in the early postnatal DS basal forebrain. Few dysregulated genes and molecular pathways were shared across cell types, suggesting that the gene expression differences in DS are largely cell-type specific. Although Hsa21 genes were slightly overrepresented when normalizing to the protein-coding genes, Hsa21-encoded genes were a small proportion of total dysregulated genes in all cell types and were largely cell-type specific. Only *PCP4*, a modulator of calcium-binding by calmodulin, emerged as a common dysregulated gene across several cell types. Functional validation of these gene expression differences will define how each cell type is affected in DS.

We uncovered two populations of BFCNs (BFCNs 1, BFCNs 2) in the early postnatal forebrain. Our findings indicate that both populations express established cholinergic marker genes, although BFCNs 2 express these genes at much lower levels.

Additionally, BFCNs 2 have increased expression of the immature neuron marker *DCX*, suggesting that this population is less mature and not fully functional. It is likely, given the early age of the samples, that BFCNs are still developing, resulting in an immature and a mature population. Both BFCN populations are present in control and DS samples. However, the DS samples have a higher proportion of the BFCNs 1 population. If the BFCNs 1 population indeed represent mature neurons, then these data align with the idea of developmental heterochrony that has been proposed in DS[69,70,72], in which development progresses precociously in DS.

Mitochondrial dysfunction and dysregulated energy metabolism are emerging as hallmarks of many neurodegenerative diseases, including those that include BFCN degeneration[61,73]. Relative to control, the more mature population of DS BFCNs upregulate several genes that encode components of the OXPHOS pathway, along with two antioxidant enzymes, *PRDX2* and *SOD1*, that detoxify reactive oxygen species (ROS) byproducts generated from OXPHOS. In response to ROS accumulation, NRF2 is activated which regulates the expression of antioxidant enzymes, including superoxide dismutases and peroxiredoxins[74]. The upregulation of these two antioxidant enzymes is potentially a compensatory mechanism to detoxify excessive ROS, further suggesting that OXPHOS is increased in DS BFCNs. We hypothesize that this early increase in energy metabolism leads to an accumulation of ROS and the resulting oxidative stress increases the vulnerability of DS BFCNs. DS BFCNs dysregulate genes associated with several neurodegenerative diseases, including AD, PD, and HD, which are characterized by mitochondrial dysfunction[61,73]. Our results suggest that dysregulated energy

metabolism and the accumulation of ROS are early events leading to the susceptibility of BFCNs in DS.

While our results indicate that dysregulated genes in DS BFCNs are associated with several neurodegenerative diseases, OXPHOS genes are typically downregulated in neurodegenerative diseases as cells shift toward glycolysis as the primary source for ATP production, a shift known as the Warburg effect[61]. Our data show that several nuclear-encoded OXPHOS subunits are upregulated in DS BFCNs, suggesting that the OXPHOS pathway is still utilized at birth in DS. In the Ts65Dn mouse model of DS and AD, OXPHOS genes are downregulated in BFCNs at 6 months of age[75,76], approximately when BFCN dysfunction and degeneration begins in this model[77,78]. The upregulation of OXPHOS genes in human early postnatal BFCNs and the downregulation in Ts65Dn 6-month BFCNs supports this potential shift in energy metabolism as these neurons begin to degenerate. The increase in genes encoding glycolytic enzymes suggests DS BFCNs may be in the early stages of shifting toward glycolysis as the primary source for energy production. A prolonged shift from OXPHOS to glycolysis can create an energy deficit that makes cells more susceptible to oxidative stress and cell death[61]. The accumulation of ROS coupled with a shift from OXPHOS to glycolysis by birth may be an early driver of BFCN vulnerability in DS.

Alternatively, the upregulation of genes encoding antioxidant enzymes and components of the glycolysis pathway may be attributed to the predominance of female samples in our study. Biological sex influences the progression of DS-AD pathogenesis[79], and sex differences have been reported in the basal forebrain cholinergic system of the Ts65Dn mouse model of DS and AD[80]. Recent spatial transcriptomic analyses of DS-AD

samples reveal that genes involved in oxidative stress and glucose metabolism are upregulated in females compared to males[81]. The upregulation of genes encoding antioxidant enzymes, the primary defense against oxidative stress, and components of the glycolysis pathway, a glucose metabolism, in our study may result from the fact that three out of four control and DS samples are from female donors. However, due to the limited availability of DS basal forebrain tissue, our study is not sufficiently powered to assess the impact of sex differences on the transcriptome of DS BFCNs.

Future studies will need to validate the shift in energy metabolism across the DS lifespan with human basal forebrain tissue and investigate the potential impact of sex differences on these metabolic changes. If these metabolic changes hold true, regulation of the OXPHOS pathway and ROS accumulation could provide a target for early therapeutic intervention in DS BFCNs prior to degeneration. It will be important to validate altered metabolism in DS cells, as fixed tissue is not amenable to analysis of dynamic metabolic processes. Induced pluripotent stem cell modeling of basal forebrain provides a paradigm for analysis[82-87]. Taken as a whole, our results reveal that metabolic dysfunction, and by extension pathology, is present in the DS basal forebrain by birth. Sustained metabolic dysregulation from birth may contribute to the susceptibility of BFCNs so early in individuals with DS.

5. References

1. Ballinger EC, Ananth M, Talmage DA, Role LW. Basal Forebrain Cholinergic Circuits and Signaling in Cognition and Cognitive Decline. *Neuron.* 2016;91(6):1199-1218.
2. Davies P, Maloney AJ. Selective loss of central cholinergic neurons in Alzheimer's disease. *Lancet.* 1976;2(8000):1403.
3. Bartus RT, Dean RL, 3rd, Beer B, Lippa AS. The cholinergic hypothesis of geriatric memory dysfunction. *Science.* 1982;217(4558):408-414.
4. Bowen DM, Smith CB, White P, Davison AN. Neurotransmitter-related enzymes and indices of hypoxia in senile dementia and other abiotrophies. *Brain.* 1976;99(3):459-496.
5. Schmitz TW, Nathan Spreng R. Basal forebrain degeneration precedes and predicts the cortical spread of Alzheimer's pathology. *Nat Commun.* 2016;7:13249.
6. Fernández-Cabello S, Kronbichler M, Van Dijk KRA, Goodman JA, Spreng RN, Schmitz TW. Basal forebrain volume reliably predicts the cortical spread of Alzheimer's degeneration. *Brain.* 2020;143(3):993-1009.
7. Schmitz TW, Mur M, Aghourian M, Bedard M-A, Spreng RN. Longitudinal Alzheimer’s Degeneration Reflects the Spatial Topography of Cholinergic Basal Forebrain Projections. *Cell Reports.* 2018;24(1):38-46.
8. Geula C, Nagykery N, Nicholas A, Wu CK. Cholinergic neuronal and axonal abnormalities are present early in aging and in Alzheimer disease. *Journal of neuropathology and experimental neurology.* 2008;67(4):309-318.

9. Moss DE, Perez RG. The phospho-tau cascade, basal forebrain neurodegeneration, and dementia in Alzheimer's disease: Anti-neurodegenerative benefits of acetylcholinesterase inhibitors. *J Alzheimers Dis.* 2024;102(3):617-626.

10. Giacobini E, Cuello AC, Fisher A. Reimagining cholinergic therapy for Alzheimer's disease. *Brain.* 2022;145(7):2250-2275.

11. Casanova MF, Walker LC, Whitehouse PJ, Price DL. Abnormalities of the nucleus basalis in Down's syndrome. *Annals of neurology.* 1985;18(3):310-313.

12. Rogers JD, Brogan D, Mirra SS. The nucleus basalis of Meynert in neurological disease: a quantitative morphological study. *Annals of neurology.* 1985;17(2):163-170.

13. Price DL, Whitehouse PJ, Struble RG, et al. Alzheimer's Disease and Down's Syndrome. *Annals of the New York Academy of Sciences.* 1982;396(1):145-164.

14. Rozalem Aranha M, Iulita MF, Montal V, et al. Basal forebrain atrophy along the Alzheimer's disease continuum in adults with Down syndrome. *Alzheimer's & dementia : the journal of the Alzheimer's Association.* 2023;19(11):4817-4827.

15. Russell JK, Conley AC, Boyd BD, et al. Age-Related Changes in the Cholinergic System in Adults with Down Syndrome Assessed Using [(18)F]-Fluoroethoxybenzovesamicol Positron Emission Tomography Imaging. *medRxiv.* 2024.

16. Candy JM, Perry RH, Perry EK, et al. Pathological changes in the nucleus of meynert in Alzheimer's and Parkinson's diseases. *Journal of the Neurological Sciences.* 1983;59(2):277-289.

17. Nakano I, Hirano A. Parkinson's disease: neuron loss in the nucleus basalis without concomitant Alzheimer's disease. *Annals of neurology.* 1984;15(5):415-418.

18. Tagliavini F, Pilleri G, Bouras C, Constantinidis J. The basal nucleus of Meynert in idiopathic Parkinson's disease. *Acta Neurol Scand.* 1984;70(1):20-28.

19. Whitehouse PJ, Hedreen JC, White CL, 3rd, Price DL. Basal forebrain neurons in the dementia of Parkinson disease. *Annals of neurology.* 1983;13(3):243-248.

20. Bohnen NI, Albin RL. The cholinergic system and Parkinson disease. *Behav Brain Res.* 2011;221(2):564-573.

21. Grothe MJ, Schuster C, Bauer F, Heinsen H, Prudlo J, Teipel SJ. Atrophy of the cholinergic basal forebrain in dementia with Lewy bodies and Alzheimer's disease dementia. *Journal of neurology.* 2014;261(10):1939-1948.

22. Lippa CF, Smith TW, Perry E. Dementia with Lewy bodies: choline acetyltransferase parallels nucleus basalis pathology. *J Neural Transm (Vienna).* 1999;106(5-6):525-535.

23. Tiraboschi P, Hansen LA, Alford M, et al. Early and Widespread Cholinergic Losses Differentiate Dementia With Lewy Bodies From Alzheimer Disease. *Archives of General Psychiatry.* 2002;59(10):946-951.

24. Schumacher J, Ray NJ, Hamilton CA, et al. Cholinergic white matter pathways in dementia with Lewy bodies and Alzheimer's disease. *Brain.* 2022;145(5):1773-1784.

25. Fortea J, Zaman SH, Hartley S, Rafii MS, Head E, Carmona-Iragui M. Alzheimer's disease associated with Down syndrome: a genetic form of dementia. *The Lancet Neurology.* 2021;20(11):930-942.

26. Lott IT, Head E. Dementia in Down syndrome: unique insights for Alzheimer disease research. *Nat Rev Neurol.* 2019;15(3):135-147.

27. Wiseman FK, Al-Janabi T, Hardy J, et al. A genetic cause of Alzheimer disease: mechanistic insights from Down syndrome. *Nature reviews Neuroscience.* 2015.

28. Kish S, Karlinsky H, Becker L, et al. Down's syndrome individuals begin life with normal levels of brain cholinergic markers. *Journal of neurochemistry.* 1989;52(4):1183-1187.

29. Brooksbank BW, Walker D, Balázs R, Jørgensen OS. Neuronal maturation in the foetal brain in Down's syndrome. *Early Hum Dev.* 1989;18(4):237-246.

30. Lubec B, Yoo BC, Dierssen M, Balic N, Lubec G. Down syndrome patients start early prenatal life with normal cholinergic, monoaminergic and serotoninergic innervation. *J Neural Transm Suppl.* 2001(61):303-310.

31. Dobin A, Davis CA, Schlesinger F, et al. STAR: ultrafast universal RNA-seq aligner. *Bioinformatics.* 2013;29(1):15-21.

32. Degatano K, Awdeh A, Dingman W, et al. WDL Analysis Research Pipelines: Cloud-Optimized Workflows for Biological Data Processing and Reproducible Analysis. *Preprints.* 2024.

33. Martin M. Cutadapt removes adapter sequences from high-throughput sequencing reads. *2011.* 2011;17(1):3.

34. Li H, Durbin R. Fast and accurate short read alignment with Burrows-Wheeler transform. *Bioinformatics.* 2009;25(14):1754-1760.

35. Zhang K, Zemke NR, Armand EJ, Ren B. A fast, scalable and versatile tool for analysis of single-cell omics data. *Nature Methods.* 2024;21(2):217-227.

36. Mathys H, Peng Z, Boix CA, et al. Single-cell atlas reveals correlates of high cognitive function, dementia, and resilience to Alzheimer's disease pathology. *Cell.* 2023;186(20):4365-4385.e4327.

37. Hao Y, Hao S, Andersen-Nissen E, et al. Integrated analysis of multimodal single-cell data. *Cell.* 2021;184(13):3573-3587.e3529.

38. Stuart T, Butler A, Hoffman P, et al. Comprehensive Integration of Single-Cell Data. *Cell.* 2019;177(7):1888-1902.e1821.

39. Young MD, Behjati S. SoupX removes ambient RNA contamination from droplet-based single-cell RNA sequencing data. *Gigascience.* 2020;9(12).

40. Gao Y, Dong Q, Arachchilage KH, et al. Multimodal analyses reveal genes driving electrophysiological maturation of neurons in the primate prefrontal cortex. *bioRxiv.* 2024.

41. McGinnis CS, Murrow LM, Gartner ZJ. DoubletFinder: Doublet Detection in Single-Cell RNA Sequencing Data Using Artificial Nearest Neighbors. *Cell Syst.* 2019;8(4):329-337.e324.

42. Wolock SL, Lopez R, Klein AM. Scrublet: Computational Identification of Cell Doublets in Single-Cell Transcriptomic Data. *Cell Syst.* 2019;8(4):281-291.e289.

43. Germain PL, Lun A, Garcia Meixide C, Macnair W, Robinson MD. Doublet identification in single-cell sequencing data using scDblFinder. *F1000Res.* 2021;10:979.

44. Korsunsky I, Millard N, Fan J, et al. Fast, sensitive and accurate integration of single-cell data with Harmony. *Nat Methods.* 2019;16(12):1289-1296.

45. Chao J, Li Z, Sun Y, et al. MG2C: a user-friendly online tool for drawing genetic maps. *Molecular Horticulture.* 2021;1(1):16.

46. Zhou Y, Zhou B, Pache L, et al. Metascape provides a biologist-oriented resource for the analysis of systems-level datasets. *Nat Commun.* 2019;10(1):1523.

47. Hao Y, Stuart T, Kowalski MH, et al. Dictionary learning for integrative, multimodal and scalable single-cell analysis. *Nature Biotechnology.* 2024;42(2):293-304.

48. Stuart T, Srivastava A, Madad S, Lareau CA, Satija R. Single-cell chromatin state analysis with Signac. *Nat Methods.* 2021;18(11):1333-1341.

49. Liu T. Use model-based Analysis of ChIP-Seq (MACS) to analyze short reads generated by sequencing protein-DNA interactions in embryonic stem cells. *Methods in molecular biology (Clifton, NJ).* 2014;1150:81-95.

50. Gaspar JM. Improved peak-calling with MACS2. *bioRxiv.* 2018:496521.

51. Takács VT, Cserép C, Schlingloff D, et al. Co-transmission of acetylcholine and GABA regulates hippocampal states. *Nature Communications.* 2018;9(1):2848.

52. Saunders A, Granger AJ, Sabatini BL. Corelease of acetylcholine and GABA from cholinergic forebrain neurons. *eLife.* 2015;4:e06412.

53. Lockstone HE, Harris LW, Swatton JE, Wayland MT, Holland AJ, Bahn S. Gene expression profiling in the adult Down syndrome brain. *Genomics.* 2007;90(6):647-660.

54. Mao R, Zielke CL, Zielke HR, Pevsner J. Global up-regulation of chromosome 21 gene expression in the developing Down syndrome brain. *Genomics.* 2003;81(5):457-467.

55. Olmos-Serrano JL, Kang HJ, Tyler WA, et al. Down Syndrome Developmental Brain Transcriptome Reveals Defective Oligodendrocyte Differentiation and Myelination. *Neuron.* 2016;89(6):1208-1222.

56. Aït Yahya-Graison E, Aubert J, Dauphinot L, et al. Classification of human chromosome 21 gene-expression variations in Down syndrome: impact on disease phenotypes. *Am J Hum Genet.* 2007;81(3):475-491.

57. Mao R, Wang X, Spitznagel EL, Jr., et al. Primary and secondary transcriptional effects in the developing human Down syndrome brain and heart. *Genome Biol.* 2005;6(13):R107.

58. Pelleri MC, Cattani C, Vitale L, et al. Integrated Quantitative Transcriptome Maps of Human Trisomy 21 Tissues and Cells. *Front Genet.* 2018;9:125-125.

59. FitzPatrick DR, Ramsay J, McGill NI, Shade M, Carothers AD, Hastie ND. Transcriptome analysis of human autosomal trisomy. *Human molecular genetics.* 2002;11(26):3249-3256.

60. Letourneau A, Santoni FA, Bonilla X, et al. Domains of genome-wide gene expression dysregulation in Down's syndrome. *Nature.* 2014;508(7496):345-350.

61. Jadiya P, Garbincius JF, Elrod JW. Reappraisal of metabolic dysfunction in neurodegeneration: Focus on mitochondrial function and calcium signaling. *Acta neuropathologica communications.* 2021;9(1):124.

62. Stevenson R, Samokhina E, Rossetti I, Morley JW, Buskila Y. Neuromodulation of Glial Function During Neurodegeneration. *Frontiers in Cellular Neuroscience.* 2020;14.

63. García O, Flores-Aguilar L. Astroglial and microglial pathology in Down syndrome: Focus on Alzheimer's disease. *Front Cell Neurosci.* 2022;16:987212.

64. Wisniewski KE, Schmidt-Sidor B. Postnatal delay of myelin formation in brains from Down syndrome infants and children. *Clinical neuropathology.* 1989;8(2):55-62.

65. Ábrahám H, Vincze A, Veszprémi B, et al. Impaired myelination of the human hippocampal formation in Down syndrome. *International Journal of Developmental Neuroscience.* 2012;30(2):147-158.

66. Santos-Pereira C, Rodrigues LR, Côrte-Real M. Emerging insights on the role of V-ATPase in human diseases: Therapeutic challenges and opportunities. *Med Res Rev.* 2021;41(4):1927-1964.

67. Mesulam MM, Mufson EJ, Levey AI, Wainer BH. Cholinergic innervation of cortex by the basal forebrain: cytochemistry and cortical connections of the septal area, diagonal band nuclei, nucleus basalis (substantia innominata), and hypothalamus in the rhesus monkey. *J Comp Neurol.* 1983;214(2):170-197.

68. Mesulam MM, Geula C. Nucleus basalis (Ch4) and cortical cholinergic innervation in the human brain: observations based on the distribution of acetylcholinesterase and choline acetyltransferase. *J Comp Neurol.* 1988;275(2):216-240.

69. Russo ML, Sousa AMM, Bhattacharyya A. Consequences of trisomy 21 for brain development in Down syndrome. *Nature reviews Neuroscience.* 2024;25(11):740-755.

70. Stagni F, Giacomini A, Emili M, Guidi S, Bartesaghi R. Neurogenesis impairment: An early developmental defect in Down syndrome. *Free Radical Biology and Medicine.* 2018;114:15-32.

71. Zdaniuk G, Wierzba-Bobrowicz T, Szpak GM, Stepien T. Astroglia disturbances during development of the central nervous system in fetuses with Down's syndrome. *Folia Neuropathol.* 2011;49(2):109-114.

72. Zhou Y, Tao L, Zhu Y. TempShift Reveals the Sequential Development of Human Neocortex and Skewed Developmental Timing of Down Syndrome Brains. *Brain Sciences.* 2023;13(7):1070.

73. Hroudová J, Singh N, Fišar Z. Mitochondrial dysfunctions in neurodegenerative diseases: relevance to Alzheimer's disease. *Biomed Res Int.* 2014;2014:175062.

74. Kasai S, Shimizu S, Tatara Y, Mimura J, Itoh K. Regulation of Nrf2 by Mitochondrial Reactive Oxygen Species in Physiology and Pathology. *Biomolecules.* 2020;10(2).

75. Alldred MJ, Lee SH, Stutzmann GE, Ginsberg SD. Oxidative Phosphorylation Is Dysregulated Within the Basocortical Circuit in a 6-month old Mouse Model of Down Syndrome and Alzheimer’s Disease. *Frontiers in Aging Neuroscience.* 2021;13.

76. Alldred MJ, Penikalapati SC, Lee SH, Heguy A, Roussos P, Ginsberg SD. Profiling Basal Forebrain Cholinergic Neurons Reveals a Molecular Basis for Vulnerability Within the Ts65Dn Model of Down Syndrome and Alzheimer's Disease. *Mol Neurobiol.* 2021;58(10):5141-5162.

77. Holtzman DM, Li YW, DeArmond SJ, et al. Mouse model of neurodegeneration: atrophy of basal forebrain cholinergic neurons in trisomy 16 transplants. *Proceedings of the National Academy of Sciences of the United States of America.* 1992;89(4):1383-1387.

78. Granholm A-CE, Sanders LA, Crnic LS. Loss of Cholinergic Phenotype in Basal Forebrain Coincides with Cognitive Decline in a Mouse Model of Down's Syndrome. *Experimental neurology.* 2000;161(2):647-663.

79. Andrews EJ, Martini AC, Head E. Exploring the role of sex differences in Alzheimer's disease pathogenesis in Down syndrome. *Frontiers in Neuroscience.* 2022;16.

80. Kelley CM, Powers BE, Velazquez R, et al. Sex differences in the cholinergic basal forebrain in the Ts65Dn mouse model of Down syndrome and Alzheimer's disease. *Brain Pathol.* 2014;24(1):33-44.

81. Miyoshi E, Morabito S, Henningfield CM, et al. Spatial and single-nucleus transcriptomic analysis of genetic and sporadic forms of Alzheimer's disease. *Nat Genet.* 2024;56(12):2704-2717.

82. Wu Y, West NR, Bhattacharyya A, Wiseman FK. Cell models for Down syndrome-Alzheimer’s disease research. *Neuronal Signaling.* 2022;6(1):NS20210054.

83. Watson LA, Meharena HS. From neurodevelopment to neurodegeneration: utilizing human stem cell models to gain insight into Down syndrome. *Front Genet.* 2023;14.

84. Muñoz SS, Engel M, Balez R, et al. A Simple Differentiation Protocol for Generation of Induced Pluripotent Stem Cell-Derived Basal Forebrain-Like Cholinergic Neurons for Alzheimer's Disease and Frontotemporal Dementia Disease Modeling. *Cells.* 2020;9(9):2018.

85. Tao R, Yue C, Guo Z, et al. Subtype-specific neurons from patient iPSCs display distinct neuropathological features of Alzheimer's disease. *Cell Regeneration.* 2024;13(1):21.

86. Hu Y, Qu Z-y, Cao S-y, et al. Directed differentiation of basal forebrain cholinergic neurons from human pluripotent stem cells. *Journal of Neuroscience Methods.* 2016;266:42-49.

87. Duan L, Bhattacharyya BJ, Belmadani A, Pan L, Miller RJ, Kessler JA. Stem cell derived basal forebrain cholinergic neurons from Alzheimer's disease patients are more susceptible to cell death. *Molecular Neurodegeneration.* 2014;9(1):3.

6. Acknowledgements

N.R.W. and A.B. would like to acknowledge the contributions of Bhattacharyya Lab members Matt Russo, Grace Branger, Kamryn Witkowiak, Rachel Lichte, and Sahith Puthireddy for their preliminary stereological analysis of the basal forebrain which played a key role in the conceptualization of this project.

7. Conflicts of Interest

The authors have no conflicts of interest to disclose.

8. Funding Sources

This study was supported by F99AG086925 from the National Institute on Aging awarded to N.R.W.; GM140935 Medical Scientist Training Program T32 from the National Institutes of Health awarded to R.D.R.; R01HD106197 from the National Institute of Child Health and Human Development awarded to A.B.; and BRFSG-2023-11 from the Brain Research Foundation awarded to A.M.M.S. Additional funding came from the William F. Vilas Trust Estate Award, Wisconsin Alzheimer's Disease Research Center Research Education Component Award, and the Wisconsin Partnership Program New Investigator Award from the University of Wisconsin-Madison to A.B.

9. Consent Statement

Acquisition of the de-identified tissue samples was approved by the Health Sciences Institutional Review Board at the University of Wisconsin-Madison (Protocol #2016-0979) and certified exempt from human subjects IRB oversight.

10. Key Words:

Down syndrome; Basal Forebrain Cholinergic Neurons (BFCNs); snMultiomic Analysis; Oxidative Phosphorylation (OXPHOS); Reactive Oxygen Species (ROS); Glycolysis

11. Figure Legends

Figure 1. A) BF samples from four control and four DS donors matched for age, sex, and PMI were used in this study. B) Schematic of BF snMultiomic analysis (Created with BioRender.com). UMAP of cell clusters by C) donor and D) age. Cells from all donors and ages are represented E) UMAP of cell clusters by subtype. Cell subtypes identified in the human basal forebrain were astrocytes, BFCNs, endothelial cells, GABAergic neurons, GPCs, microglia, oligodendrocytes, and OPCs.

Figure 2. A) UMAP of cell clusters by subtype split by control and DS. Proportion of cell types in control (N=20,826) and DS (N=16,641). There are fewer astrocytes and more GABAergic neurons and microglia in the DS basal forebrain. B) PCA analysis of cell type and genotype. Cell types from control and DS are largely the same, with control and DS clustering together on the plot. Cells cluster by subclass. C) DEGs for astrocytes, BFCNs, GABAergic neurons, microglia, and oligodendrocytes are distributed across the genome. D) KEGG pathway analysis showing gene enrichment. DEGs in BFCNs enriched in 'Glycolysis and Gluconeogenesis' pathways.

Figure 3. A) Chromosome map of Hsa21 DEGs color-coded by cell type. B) Percent of Hsa21 DEGs relative to total DEGs per cell type. C) Volcano plot of dysregulated Hsa21 genes in DS astrocytes. DS astrocytes upregulate 31 Hsa21 genes. D) Volcano plot of dysregulated Hsa21 genes in DS BFCNs. DS BFCNs upregulate 11 Hsa21 genes. E) Volcano plot of dysregulated Hsa21 genes in DS GABAergic neurons. DS GABAergic neurons upregulate 19 Hsa21 genes. F) Volcano plot of dysregulated Hsa21 genes in

DS microglia. DS microglia upregulate four and downregulate two Hsa21 genes. G) Volcano plot of dysregulated Hsa21 genes in DS oligodendrocytes. DS oligodendrocytes upregulate eight and downregulate two Hsa21 genes. H) Percent of Hsa21 DEGs normalized to total protein-coding genes per cell type.

Figure 4. A) Multiomic UMAP of cell clusters by subtype split by control and DS. B) Chromatin accessibility and peak-to-gene linkages for *DSCAM* and *S100B* in control and DS astrocytes. C) Chromatin accessibility and peak-to-gene linkages for *PCP4* and *SOD1* in control and DS GABAergic neurons. D) Chromatin accessibility and peak-to-gene linkages for *EVA1C* and *S100B* in control and DS microglia. E) Chromatin accessibility and peak-to-gene linkages for *FTCD* and *IFNGR2* in control and DS oligodendrocytes. All of these genes have larger peaks around the TSS in DS, suggesting increased chromatin accessibility in the promoter region of each gene within the respective cell type.

Figure 5. A) The Glial subclass was subset and reclustered. UMAP of cell clusters by subtype split by control and DS. Proportion of glial subtypes in control and DS. B) Percent of DEGs normalized to protein-coding genes per chromosome in DS astrocytes with Hsa21 highlighted in red. Top 30 DEGs in DS astrocytes. C) KEGG pathway analysis of enriched genes in control and DS astrocytes. DS astrocyte DEGs are enriched in ‘Regulation of Actin Cytoskeleton’ and ‘Fc Gamma R-Mediated Phagocytosis’ pathways D) Percent of DEGs normalized to protein-coding genes per chromosome in DS microglia with Hsa21 highlighted in red. Top 30 DEGs in DS microglia. E) KEGG pathway analysis of enriched genes in control and DS microglia. DS microglia DEGs are enriched for genes

involved in the ‘Leishmania Infection’ pathway F) Percent of DEGs normalized to protein-coding genes per chromosome in DS oligodendrocytes with Hsa21 highlighted in red. Top 30 DEGs in DS oligodendrocytes. G) KEGG pathway analysis of enriched genes in control and DS oligodendrocytes. There are genes enriched in the ‘Oxidative Phosphorylation’ pathway in DS oligodendrocytes.

Figure 6. A) The GABAergic subclass was subset and reclustered. UMAP of cell clusters by subtype split by control and DS. Proportion of GABAergic subtypes in control and DS. B) Top 30 markers identified in BFCNs relative to GABAergic neurons. C) Percent of DEGs normalized to protein-coding genes per chromosome in DS GABAergic neurons with Hsa21 highlighted in red. D) Volcano plot of dysregulated genes in DS GABAergic neurons. E) Top 30 DEGs in DS GABAergic neurons. F) KEGG pathway analysis of enriched genes in control and DS GABAergic neurons. Genes involved in the ‘Oxidative Phosphorylation’ pathway and genes associated with ‘Alzheimer’s Disease’ are enriched in DS GABAergic neurons G) Percent of DEGs normalized to protein-coding genes per chromosome in DS BFCNs with Hsa21 highlighted in red. H) Volcano plot of dysregulated genes in DS BFCNs. I) Top 30 DEGs in DS BFCNs. J) KEGG pathway analysis of enriched genes in control and DS BFCNs. In DS BFCNs, DEGs are enriched in the ‘Oxidative Phosphorylation’ pathway and genes associated with neurodegenerative diseases, including ‘Huntington’s Disease’ and ‘Parkinson’s Disease’.

Figure 7. A) BFCNs were subset from the data and re-clustered. UMAP of cell clusters by BFCN subpopulation split by control and DS. Two distinct clusters are present in the

UMAP of BFCNs. These two clusters were annotated as BFCNs 1 and BFCNs 2. Proportion of BFCN subpopulations in control and DS. B) Expression of known cholinergic marker genes in BFCN subpopulations. BFCNs 2 have lower expression of most of these genes in both control and DS. C) Expression of immature and mature neuron marker genes in BFCN subpopulations. BFCNs 1 have higher expression of mature neuron marker genes while BFCNs 2 have more expression of immature neuron marker genes. D) Top 30 DEGs between BFCNs 1 and BFCNs 2. E) KEGG pathway analysis of enriched genes in BFCNs 1 and BFNCs 2. BFCNs 1 DEGs are enriched for genes involved in 'Oxidative Phosphorylation' and 'Glycolysis and Gluconeogenesis' pathways. F) BFCNs 1 DEGs between DS and control. DS BFCNs 1 have 49 dysregulated genes. G) Percent of DEGs normalized to protein-coding genes per chromosome in DS BFCNs 1 with Hsa21 highlighted in red. H) BFCNs 2 DEGs between DS and control. DS BFCNs 2 have 5 dysregulated genes. I) Percent of DEGs normalized to protein-coding genes per chromosome in DS BFCNs 2. J) PCA analysis of BFCN subpopulations and genotype. Separation of control and DS BFCNs 1 confirm they are more dissimilar compared to control and DS BFCNs 2 which cluster close together.

Figure 8. A) Top 30 DEGs in DS BFCNs 1. B) GO Term enrichment analysis of genes upregulated in DS BFCNs 1. Upregulated genes in DS BFCNs are enriched for the 'Cellular Process' and 'Homeostatic Process' categories C) KEGG pathway analysis of enriched genes in control and DS BFCNs 1. In DS BFCNs 1, DEGs are enriched in the 'Oxidative Phosphorylation' pathway and genes associated with 'Parkinson's Disease'. D) CNA of upregulated genes in DS BFCNs 1. Dysregulated BFCNs 1 genes are enriched

‘Oxidative Phosphorylation’ and ‘Glycolysis and Gluconeogenesis’ pathways and are associated with several neurodegenerative diseases. E) Chromatin accessibility for *PRDX2*, *ATP6V0C,* and *SOD1* in control and DS BFCNs 1. There is increased chromatin accessibility in the promoter regions of *PRDX2* and *ATP6V0C* in DS BFCNs 1 but no difference in chromatin accessibility in the promoter region of *SOD1*.

Figure 1

A.

Tissue Samples				
Subject	**Condition**	**Sex**	**Age**	**PMI (hrs)**
4901	Control	Female	61 days	28
5987	DS	Female	65 days	28
4239	Control	Female	52 days	36
4457	DS	Female	185 days	32
5655	Control	Female	91 days	28
1282	DS	Female	186 days	28
1063	Control	Male	1 yr 123 days	21
714	DS	Male	1 yr 319 days	17

B.

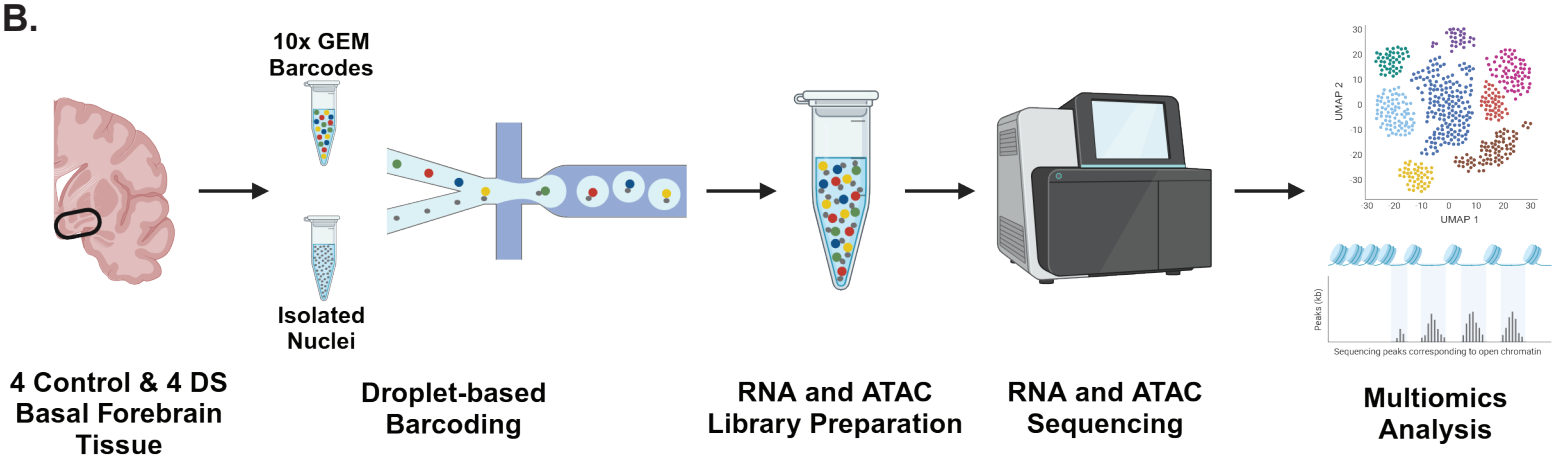

C.

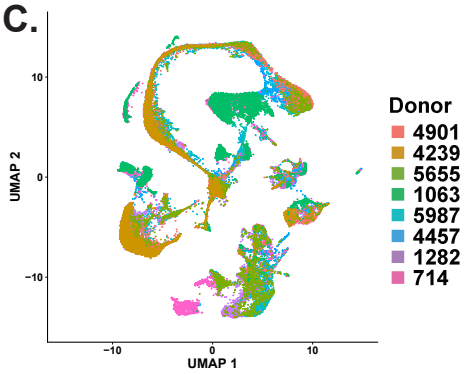

D.

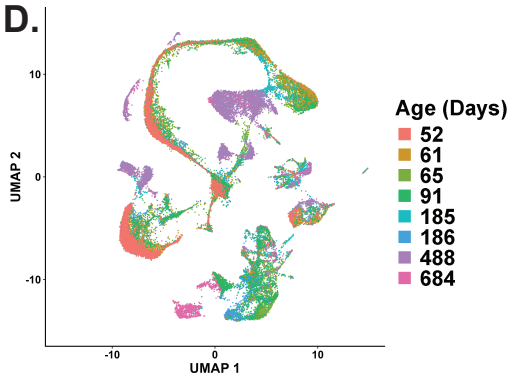

E.

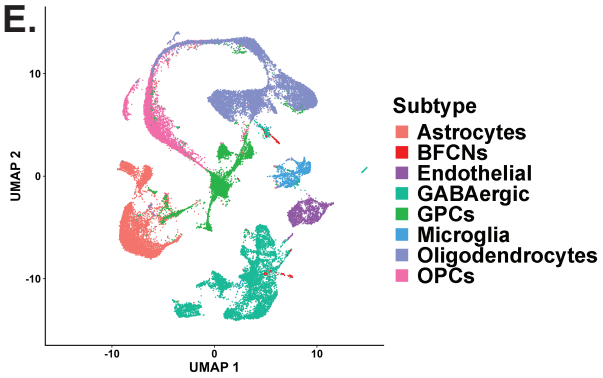

Figure 2

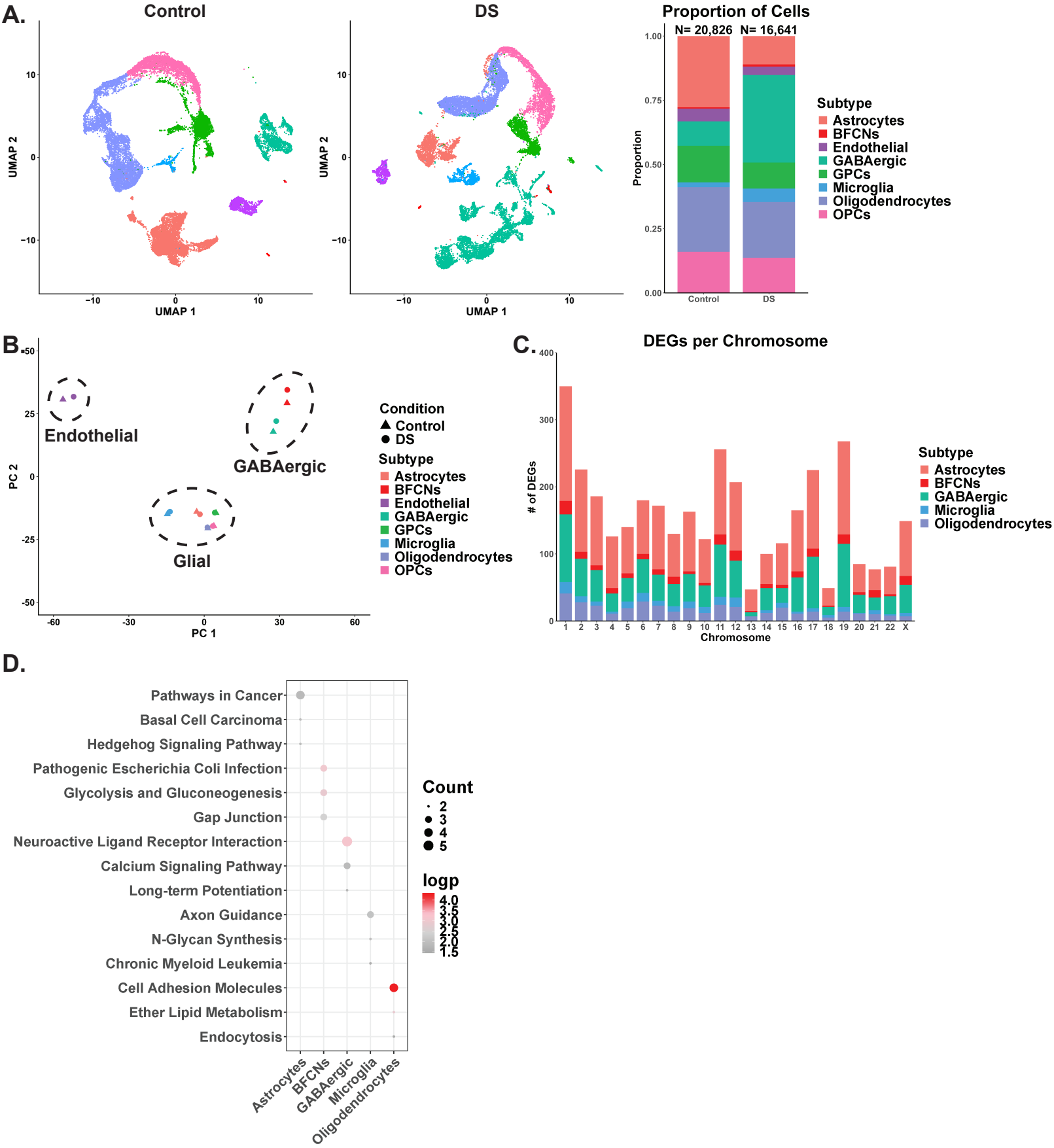
A.
Control
DS
Proportion of Cells
N= 20,826
N= 16,641
UMAP 1
UMAP 2
Proportion
Control
DS
Subtype
Astrocytes
BFCNs
Endothelial
GABAergic
GPCs
Microglia
Oligodendrocytes
OPCs
B.
Endothelial
GABAergic
Glial
PC 1
PC 2
Condition
Control
DS
Subtype
Astrocytes
BFCNs
Endothelial
GABAergic
GPCs
Microglia
Oligodendrocytes
OPCs
C.
DEGs per Chromosome
# of DEGs
Chromosome
Subtype
Astrocytes
BFCNs
GABAergic
Microglia
Oligodendrocytes
D.
Pathways in Cancer
Basal Cell Carcinoma
Hedgehog Signaling Pathway
Pathogenic Escherichia Coli Infection
Glycolysis and Gluconeogenesis
Gap Junction
Neuroactive Ligand Receptor Interaction
Calcium Signaling Pathway
Long-term Potentiation
Axon Guidance
N-Glycan Synthesis
Chronic Myeloid Leukemia
Cell Adhesion Molecules
Ether Lipid Metabolism
Endocytosis
Astrocytes
BFCNs
GABAergic
Microglia
Oligodendrocytes
Count
2
3
4
5
logp
4.0
3.5
3.0
2.5
2.0
1.5

Figure 3

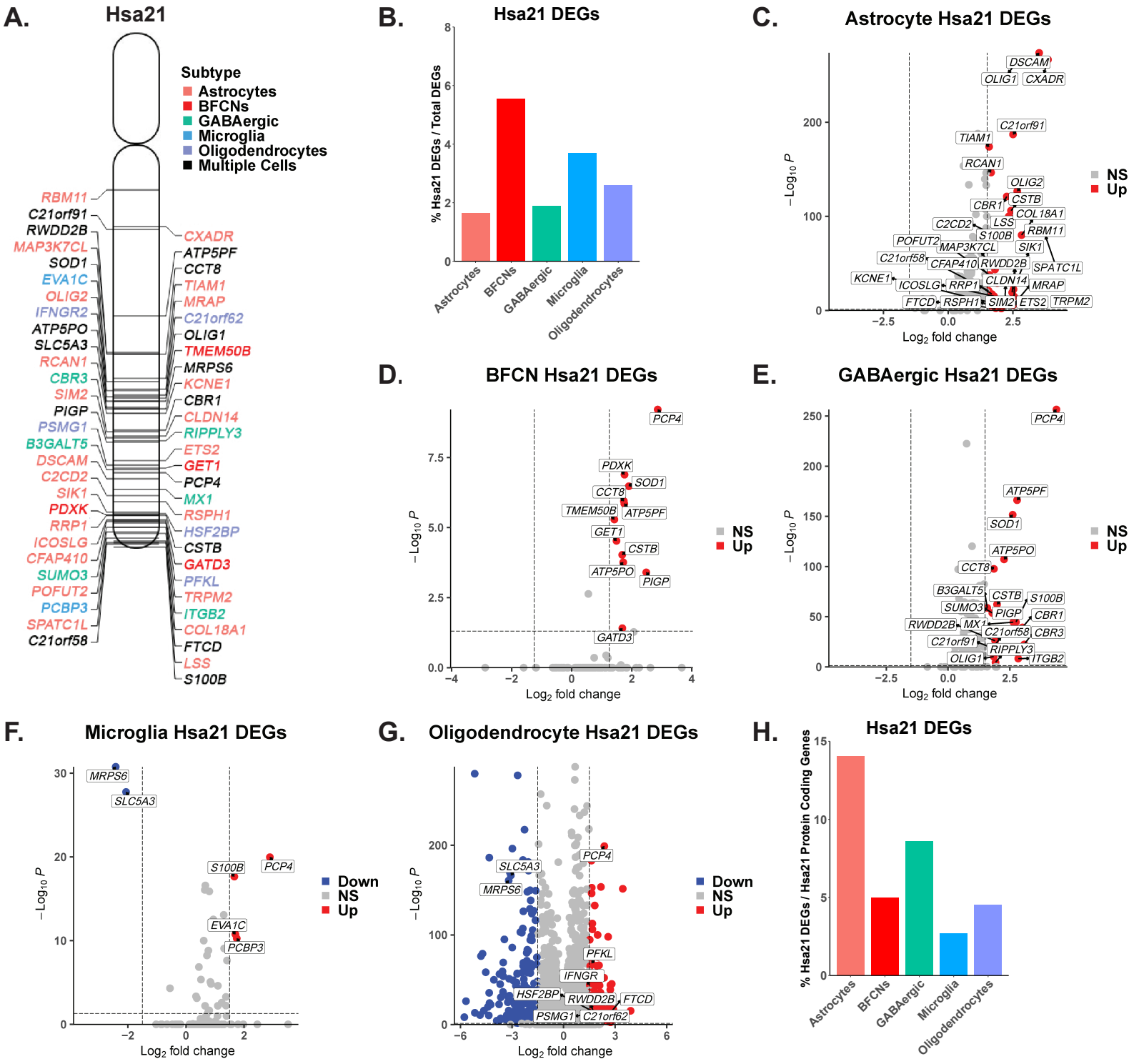
A.
Hsa21
Subtype
Astrocytes
BFCNs
GABAergic
Microglia
Oligodendrocytes
Multiple Cells
RBM11
C21orf91
RWDD2B
MAP3K7CL
SOD1
EVA1C
OLIG2
IFNGR2
ATP5PO
SLC5A3
RCAN1
CBR3
SIM2
PIGP
PSMG1
B3GALT5
DSCAM
C2CD2
SIK1
PDXK
RRP1
ICOSLG
CFAP410
SUMO3
POFUT2
PCBP3
SPATC1L
C21orf58
CXADR
ATP5PF
CCT8
TIAM1
MRAP
C21orf62
OLIG1
TMEM50B
MRPS6
KCNE1
CBR1
CLDN14
RIPPLY3
ETS2
GET1
PCP4
MX1
RSPH1
HSF2BP
CSTB
GATD3
PFKL
TRPM2
ITGB2
COL18A1
FTCD
LSS
S100B
B.
Hsa21 DEGs
% Hsa21 DEGs / Total DEGs
Astrocytes
BFCNs
GABAergic
Microglia
Oligodendrocytes
C.
Astrocyte Hsa21 DEGs
−Log10 P
Log2 fold change
NS
Up
D.
BFCN Hsa21 DEGs
E.
GABAergic Hsa21 DEGs
F.
Microglia Hsa21 DEGs
Down
NS
Up
G.
Oligodendrocyte Hsa21 DEGs
H.
Hsa21 DEGs
% Hsa21 DEGs / Hsa21 Protein Coding Genes

Figure 4

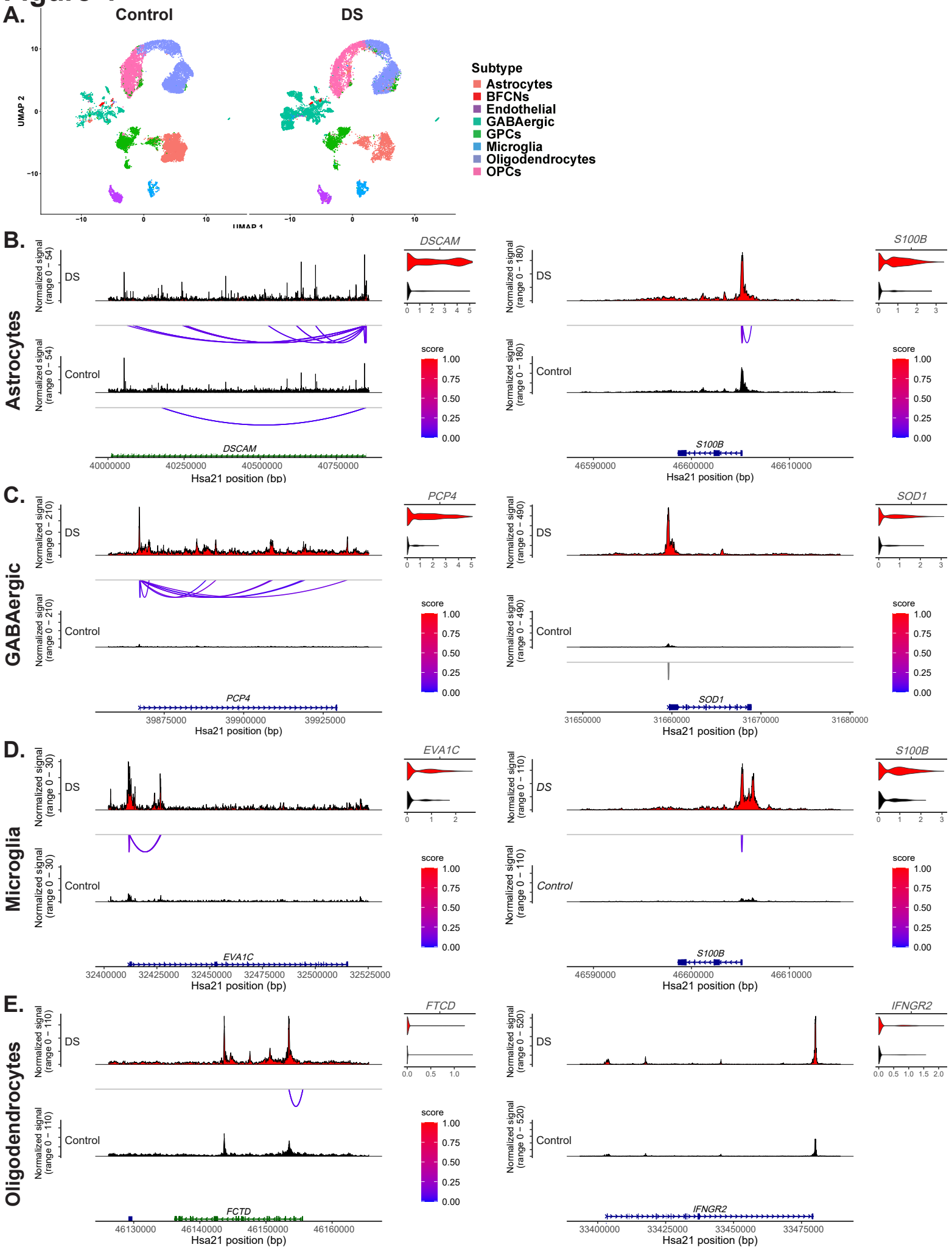
A.
Control
DS
UMAP 2
UMAP 1
Subtype
Astrocytes
BFCNs
Endothelial
GABAergic
GPCs
Microglia
Oligodendrocytes
OPCs
B.
Astrocytes
DSCAM
S100B
DS
Control
Normalized signal (range 0 – 54)
Normalized signal (range 0 – 180)
score
Hsa21 position (bp)
C.
GABAergic
PCP4
SOD1
Normalized signal (range 0 – 210)
Normalized signal (range 0 – 490)
D.
Microglia
EVA1C
S100B
Normalized signal (range 0 – 30)
Normalized signal (range 0 – 110)
E.
Oligodendrocytes
FTCD
IFNGR2
Normalized signal (range 0 – 110)
Normalized signal (range 0 – 520)

Figure 5

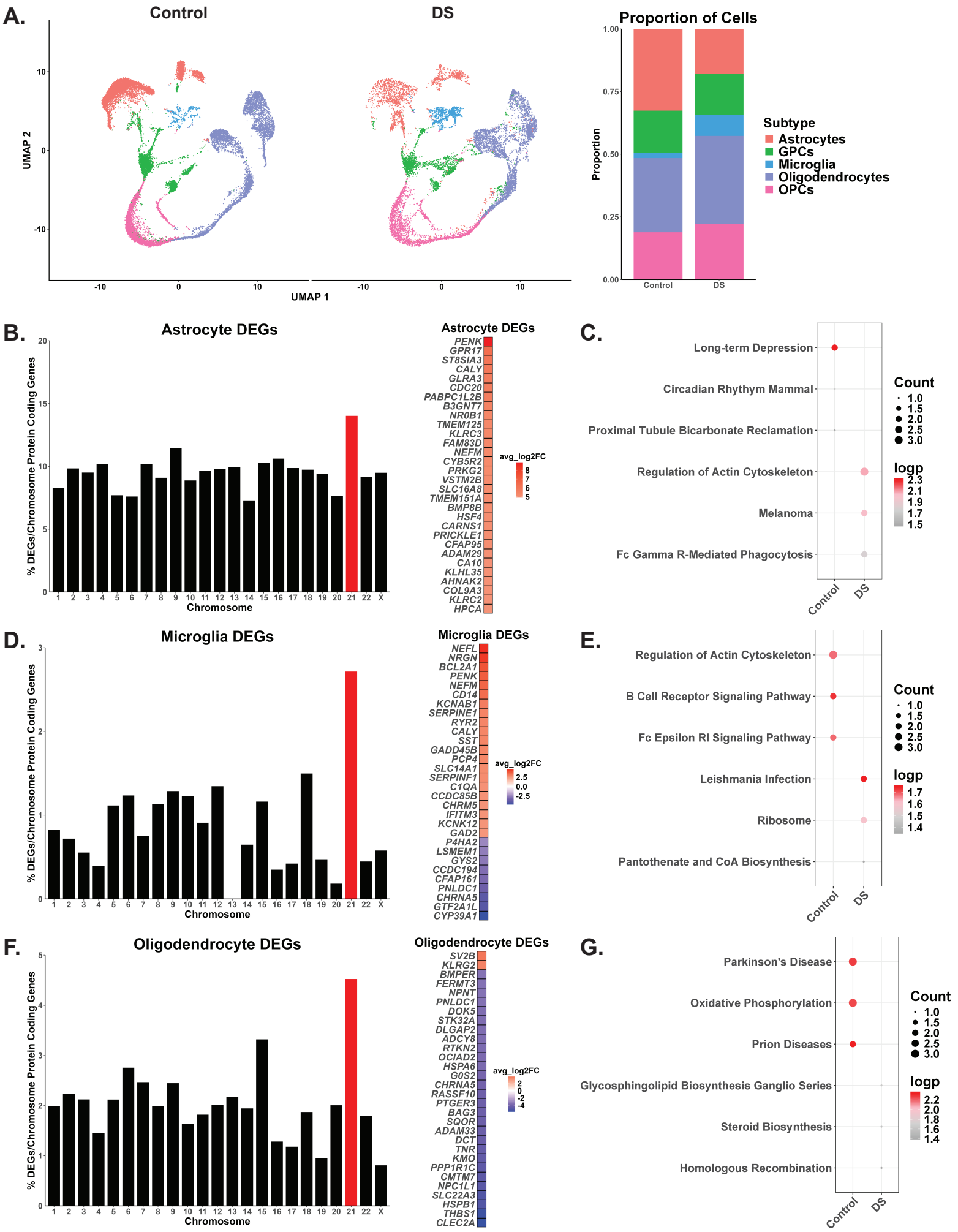
A.
Control
DS
UMAP 2
UMAP 1
Proportion of Cells
Proportion
Control
DS
Subtype
Astrocytes
GPCs
Microglia
Oligodendrocytes
OPCs
B.
Astrocyte DEGs
% DEGs/Chromosome Protein Coding Genes
Chromosome
Astrocyte DEGs
PENK
GPR17
ST8SIA3
CALY
GLRA3
CDC20
PABPC1L2B
B3GNT7
NR0B1
TMEM125
KLRC3
FAM83D
NEFM
CYB5R2
PRKG2
VSTM2B
SLC16A8
TMEM151A
BMP8B
HSF4
CARNS1
PRICKLE1
CFAP95
ADAM29
CA10
KLHL35
AHNAK2
COL9A3
KLRC2
HPCA
avg_log2FC
C.
Long-term Depression
Circadian Rhythm Mammal
Proximal Tubule Bicarbonate Reclamation
Regulation of Actin Cytoskeleton
Melanoma
Fc Gamma R-Mediated Phagocytosis
Control
DS
Count
logp
D.
Microglia DEGs
% DEGs/Chromosome Protein Coding Genes
Chromosome
Microglia DEGs
NEFL
NRGN
BCL2A1
PENK
NEFM
CD14
KCNAB1
SERPINE1
RYR2
CALY
SST
GADD45B
PCP4
SLC14A1
SERPINF1
C1QA
CCDC85B
CHRM5
IFITM3
KCNK12
GAD2
P4HA2
LSMEM1
GYS2
CCDC194
CFAP161
PNLDC1
CHRNA5
GTF2A1L
CYP39A1
avg_log2FC
E.
Regulation of Actin Cytoskeleton
B Cell Receptor Signaling Pathway
Fc Epsilon RI Signaling Pathway
Leishmania Infection
Ribosome
Pantothenate and CoA Biosynthesis
Control
DS
Count
logp
F.
Oligodendrocyte DEGs
% DEGs/Chromosome Protein Coding Genes
Chromosome
Oligodendrocyte DEGs
SV2B
KLRG2
BMPER
FERMT3
NPNT
PNLDC1
DOK5
STK32A
DLGAP2
ADCY8
RTKN2
OCIAD2
HSPA6
G0S2
CHRNA5
RASSF10
PTGER3
BAG3
SQOR
ADAM33
DCT
TNR
KMO
PPP1R1C
CMTM7
NPC1L1
SLC22A3
HSPB1
THBS1
CLEC2A
avg_log2FC
G.
Parkinson's Disease
Oxidative Phosphorylation
Prion Diseases
Glycosphingolipid Biosynthesis Ganglio Series
Steroid Biosynthesis
Homologous Recombination
Control
DS
Count
logp

Figure 6

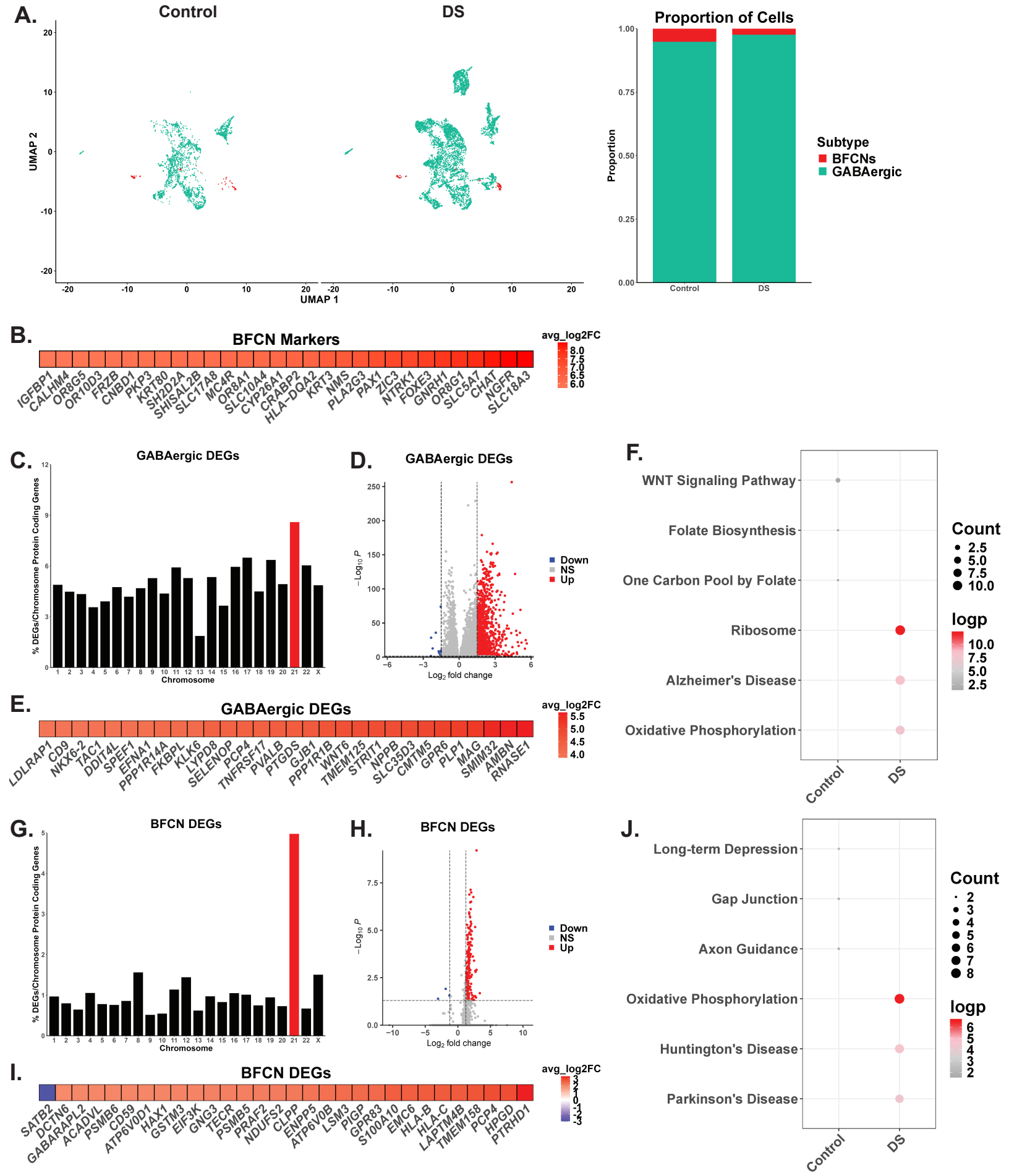
A.
Control
DS
UMAP 2
UMAP 1
Proportion of Cells
Proportion
Control
DS
Subtype
BFCNs
GABAergic
B.
BFCN Markers
avg_log2FC
IGFBP1
CALHM4
OR8G5
OR10D3
FRZB
CNBD1
PKP3
KRT80
SH2D2A
SHISAL2B
SLC17A8
MC4R
OR8A1
SLC10A4
CYP26A1
CRABP2
HLA-DQA2
KRT3
NMS
PLA2G3
PAX1
ZIC3
NTRK1
FOXE3
GNRH1
OR8G1
SLC5A7
CHAT
NGFR
SLC18A3
C.
GABAergic DEGs
% DEGs/Chromosome Protein Coding Genes
Chromosome
D.
GABAergic DEGs
Log2 fold change
Down
NS
Up
F.
WNT Signaling Pathway
Folate Biosynthesis
One Carbon Pool by Folate
Ribosome
Alzheimer's Disease
Oxidative Phosphorylation
Control
DS
Count
logp
E.
GABAergic DEGs
avg_log2FC
LDLRAP1
CD9
NKX6-2
TAC1
DDIT4L
SPEF1
EFNA1
PPP1R14A
FKBPL
KLK6
LYPD8
SELENOP
PCP4
TNFRSF17
PVALB
PTGDS
GJB1
PPP1R1B
WNT6
TMEM125
STRIT1
NPPB
SLC35D3
CMTM5
GPR6
PLP1
MAG
SMIM32
AMBN
RNASE1
G.
BFCN DEGs
% DEGs/Chromosome Protein Coding Genes
Chromosome
H.
BFCN DEGs
Log2 fold change
Down
NS
Up
J.
Long-term Depression
Gap Junction
Axon Guidance
Oxidative Phosphorylation
Huntington's Disease
Parkinson's Disease
Control
DS
Count
logp
I.
BFCN DEGs
avg_log2FC
SATB2
DCTN6
GABARAPL2
ACADVL
PSMB6
CD59
ATP6V0D1
HAX1
GSTM3
EIF3K
GNG3
TECR
PSMB5
PRAF2
NDUFS2
CLPP
ENPP5
ATP6V0B
LSM3
PIGP
GPR83
S100A10
EMC6
HLA-B
HLA-C
LAPTM4B
TMEM158
PCP4
HPGD
PTRHD1

Figure 7

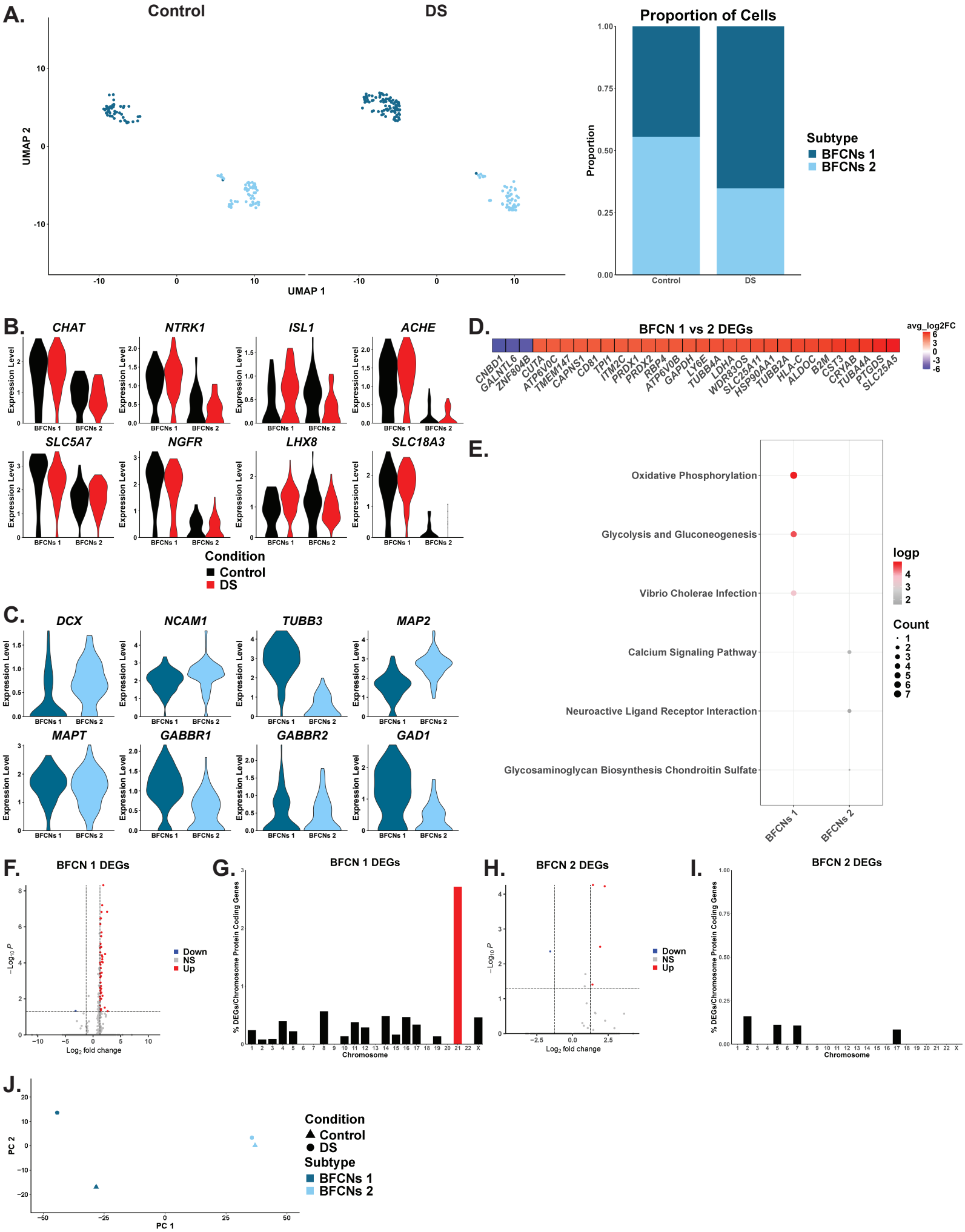
A.
Control
DS
UMAP 2
UMAP 1
Proportion of Cells
Proportion
Control
DS
Subtype
BFCNs 1
BFCNs 2
B.
CHAT
NTRK1
ISL1
ACHE
SLC5A7
NGFR
LHX8
SLC18A3
Expression Level
BFCNs 1
BFCNs 2
Condition
Control
DS
C.
DCX
NCAM1
TUBB3
MAP2
MAPT
GABBR1
GABBR2
GAD1
D.
BFCN 1 vs 2 DEGs
avg_log2FC
CNBD1
GALNTL6
ZNF804B
CUTA
ATP6V0C
TMEM147
CAPNS1
CD81
TPI1
ITM2C
PRDX1
PRDX2
RBP4
ATP6V0B
GAPDH
LY6E
TUBB4A
LDHA
WDR83OS
SLC25A11
HSP90AA1
TUBB2A
HLA-C
ALDOC
B2M
CST3
CRYAB
TUBA4A
PTGDS
SLC25A5
E.
Oxidative Phosphorylation
Glycolysis and Gluconeogenesis
Vibrio Cholerae Infection
Calcium Signaling Pathway
Neuroactive Ligand Receptor Interaction
Glycosaminoglycan Biosynthesis Chondroitin Sulfate
logp
Count
BFCNs 1
BFCNs 2
F.
BFCN 1 DEGs
Down
NS
Up
Log2 fold change
G.
BFCN 1 DEGs
% DEGs/Chromosome Protein Coding Genes
Chromosome
H.
BFCN 2 DEGs
Down
NS
Up
Log2 fold change
I.
BFCN 2 DEGs
% DEGs/Chromosome Protein Coding Genes
Chromosome
J.
PC 1
PC 2
Condition
Control
DS
Subtype
BFCNs 1
BFCNs 2

Figure 8

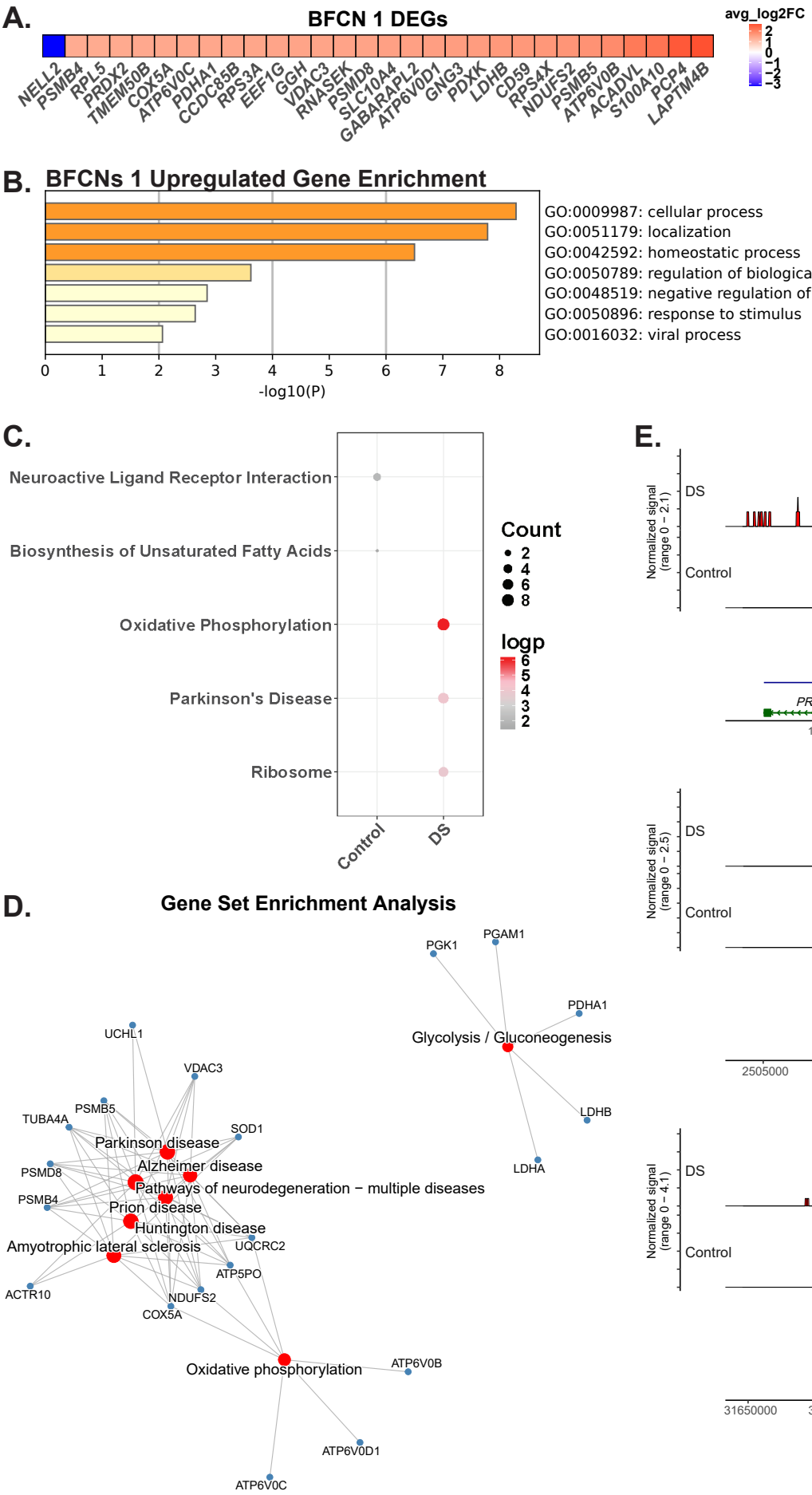
A.
BFCN 1 DEGs
avg_log2FC
2
1
0
−1
−2
−3
NELL2
PSMB4
RPL5
PRDX2
TMEM50B
COX5A
ATP6V0C
PDHA1
CCDC85B
RPS3A
EEF1G
GGH
VDAC3
RNASEK
PSMD8
SLC10A4
GABARAPL2
ATP6V0D1
GNG3
PDXK
LDHB
CD59
RPS4X
NDUFS2
PSMB5
ATP6V0B
ACADVL
S100A10
PCP4
LAPTM4B
B.
BFCNs 1 Upregulated Gene Enrichment
GO:0009987: cellular process
GO:0051179: localization
GO:0042592: homeostatic process
GO:0050789: regulation of biological process
GO:0048519: negative regulation of biological process
GO:0050896: response to stimulus
GO:0016032: viral process
0
1
2
3
4
5
6
7
8
-log10(P)
C.
Neuroactive Ligand Receptor Interaction
Biosynthesis of Unsaturated Fatty Acids
Oxidative Phosphorylation
Parkinson's Disease
Ribosome
Control
DS
Count
2
4
6
8
logp
6
5
4
3
2
D.
Gene Set Enrichment Analysis
PGK1
PGAM1
PDHA1
Glycolysis / Gluconeogenesis
LDHB
LDHA
UCHL1
VDAC3
PSMB5
TUBA4A
SOD1
Parkinson disease
Alzheimer disease
PSMD8
Pathways of neurodegeneration − multiple diseases
PSMB4
Prion disease
Huntington disease
Amyotrophic lateral sclerosis
UQCRC2
ATP5PO
ACTR10
NDUFS2
COX5A
Oxidative phosphorylation
ATP6V0B
ATP6V0D1
ATP6V0C
E.
PRDX2
DS
Control
Normalized signal
(range 0 – 2.1)
0
1
2
3
PRDX2
12800000
12805000
12810000
Hsa19 position (bp)
ATP6V0C
DS
Control
Normalized signal
(range 0 – 2.5)
0
1
2
3
ATP6V0C
2505000
2510000
2515000
2520000
Hsa16 position (bp)
SOD1
DS
Control
Normalized signal
(range 0 – 4.1)
0
1
2
3
SOD1
31650000
31655000
31660000
31665000
31670000
Hsa21 position (bp)